

**FABRICATION, CHARACTERIZATION AND
APPLICATION
OF ZINC OXIDE THIN FILM NANOROD
IN DYE-SENSITIZED SOLAR CELLS AND GAS
SENSORS**



A

Dissertation Submitted to the Central Department of Physics,
Institute of Science and Technology,
Tribhuvan University, Nepal
for the Award of
Doctor of Philosophy (Ph.D.) Degree in Physics

By

Indra Bahadur Karki

2013 AD (2070 BS)

Outline of Thesis

Title Page	i
Recommendation	iii
Certificate of Approval	iv
Acknowledgement	v
Affirmation of Independent Work	vi
Abstract	vii
Table of Content	ix
List of Abbreviations	xv

RECOMMENDATION

This is to certify that **Mr. Indra Bahadur Karki** has completed this dissertation work entitled **Fabrication, Characterization and Application of ZnO Thin Films Nanorod in Dye-Sensitized Solar Cells (DSSCs) and Gas Sensors** for the award of **Doctor of Philosophy in Physics** under our supervision. To our knowledge, this work has not been submitted for any other degree.

.....

Dr. Suman Chatterjee
Co-Supervisor
Department of Physics,
North Bengal University, Siliguri,
West Bengal, India

Date:.....

.....

Prof. Dr. Jeevan Jyoti Nakarmi
Supervisor
Central Department of Physics,
Tribhuvan University, Kirtipur
Kathmandu, Nepal

Date:.....

CERTIFICATE OF APPROVAL

On the recommendation of **Prof. Dr. Lok Narayan Jha**, this dissertation work of **Mr. Indra Bahadur Karki** is forwarded for the examination and is submitted to the IOST, Tribhuvan University for the award of **Doctor of Philosophy (Ph. D.) Degree in Physics**.

.....

Head

Central Department of Physics,
Tribhuvan University, Kirtipur,
Kathmandu, Nepal

Date:

ACKNOWLEDGEMENTS

My first and foremost thanks go to my eminent supervisor Prof. Dr. Jeevan Jyoti Nakarmi for providing me this precious opportunity to work with him, his guidance and input throughout the process of this research. Sincere appreciation goes to my co-supervisor Dr. Suman Chatterjee for his suggestions and invaluable help of constructive comments throughout this work that have contributed greatly to the success of this research.

My deepest gratitude goes also to Prof. Dr. P K Mandal for his endless support and for providing laboratory facilities during my research work. I am heartedly grateful to Prof. Dr. A. Mukhopadhyay (Dean and HOD, Department of Physics, North Bengal University) for his cooperation and good wishes. I wish to mention deep sense of gratitude towards Prof. Dr. Lok Narayan Jha for his valuable suggestions during the research period. I am also thankful to Prof. Dr. O P Niroula, Dr. N P Adhikari, Dr. Nawa Raj Khatiwada, Ms. Dimple Jhelumi, Mr. D. Sinha, Mr. Devargo for their helpful discussions and encouragement. I would like to thank the UGC, Bhaktapur for PhD fellowship and to pay my sincere thanks to NAST, Nepal and INSA, India for their partial financial support to PhD research work.

I am also thankful to all of my NBU hostel members for their cooperation and nice company. I would like to express my profound admiration and salute to my father Mr. Ganja Bahadur Karki and my mother Mrs. Chandra Kumari Karki. I would essentially have not been able to achieve this noble goal without their help and kindness.

Finally, heartfelt thanks go to my beloved wife Jagjit Kour and sweet children Ms. Kshitiz and Aashutosh for their endless support, enormous love and patience throughout the course of my studies. Words are hardly enough to express my gratitude to all of them and their endurance for my PhD studies.

- Indra Bahadur Karki

AFFIRMATION OF INDEPENDENT WORK

I hereby certify that this material which I now submit for assessment on the programme of study leading to the award of Doctor of Philosophy in Physics is entirely my own work. I have exercised reasonable care to ensure that the work is original, and does not to the best of my knowledge breach any law of copyright, and has not been taken from the work of others save and to the extent that such work has been cited and acknowledged within the text of my work.

Signed: _____

ID No.: 73/2009, Dean's

Office, IOST, T.U., Kirtipur.

ABSTRACT

Multifunctional zinc oxide (ZnO) semiconductor is a potential candidate for electronics and optoelectronics applications and can be utilized commercially due to its availability, chemical stability and other excellent electrical and optical properties. The semiconducting and piezoelectric properties of environmental friendly ZnO are extremely useful for designing new kind of energy harvesting devices. As a part of this PhD work, an extensive research were performed on ZnO based materials, both as nano powders and thin films that relates specifically to ZnO nanostructure based electrochemical sensors and Dye-Sensitized Solar Cells (DSSCs) applications.

The research focused on the synthesis and characterization of zinc oxide thin films. The thin films were prepared using sol-gel spin coating method (thin film deposition) while the structural characterization of the films was performed by X-ray diffraction and the morphology was evaluated by SEM Microscopy. The electrical properties of the ZnO thin films based DSSCs were determined by Keithley 2400 digital multimeter and absorption spectra of natural dyes were determined through UV-VIS spectroscopy.

One of the main objectives of this experimental research work is to study alternative locally available low-cost natural dye for DSSCs. In comparison to the more common Anthocyanin and Xanthene type natural dyes extracted from fruit extracts was also investigated. Following the recent developments in low cost materials and techniques for electrochemical solar cells using natural dyes and its properties and application based on the ZnO nanorod structures, the influence of various preparation parameters: dyes, temperature we have investigated and *I-V* characteristics of DSSCs were investigated. The characterization of the obtained ZnO nanostructures has been performed by using X-ray diffraction, SEM.

Another main objective of this research work is to analyze sensing behaviour of zinc oxide nanorod substrate as a resistive sensor for Volatile Organic Components (VOC). The application of fabricated devices was successfully demonstrated as chemical sensors for the detection of tea aroma using potentiometric technique. The sensor devices fabricated and characterized in the work were used to detect tea aroma of Darjeeling Orthodox and Assam, India, CTC tea.

ZnO nanorod layers doped with various dopants were characterized individually for application as sensing element and finally, these sensors were assembled in the form of an electronic nose (E-nose). This e-nose assembly was tested for detection of tea aroma. Tea aroma is the resultant of various organic volatile molecules, which determine the quality of tea. Finally, a standardized device was fabricated for determining quality of tea based upon its aroma.

TABLE OF CONTENTS

CHAPTER 1 INTRODUCTION	1
1.2 Nanotechnology and Nano devices	1
1.2 Dye Sensitized Solar Cells	4
1.2.1 Problems in Fossil Fuels – need for alternative source	4
1.2.2 Harvesting solar energy	5
1.2.3 Solar Photovoltaic Cells	6
1.2.4 State of the Art in Solar Cells	8
1.3 Sensor Materials	15
1.3.1 Challenges in Sensors	15
1.3.2 State of the Art in Sensing materials	16
CHAPTER 2 OBJECTIVES	18
CHAPTER 3 LITERATURE REVIEW	20
3.1 Nano devices and Nanostructured sensing elements	20
3.2 ZnO Nanorods	20
3.2.1 The ZnO nanorods and its properties	20
3.2.2 Doping of nanostructured ZnO	22
3.3 Dye Sensitized Solar Cells	25
3.3.1 Harvesting Solar Power: Solar Cells	25
3.4 Operational Principles of Dye-sensitized solar cells	29
3.4.1 The dye: light harvesting and charge separation	32

3.4.2	The electrolyte: regeneration of the dye and hole conduction	34
3.4.3	The counter electrode: regeneration of the oxidized species in the electrolyte	36
3.4.4	The mesoporous semiconductor: ZnO as electron conductor in DSSCs	37
3.5	Theoretical description of dye-sensitized solar cells	37
3.5.1	Current-voltage characteristics	37
3.5.2	Electron recombination and the origin of the photovoltage in DSSCs	40
3.5.3	Photocurrent and incident photon to current efficiency	47
3.6	Gas Sensors	48
3.6.1	ZnO based Gas Sensor	48
3.6.2	Detection of Tea Aroma	49
3.6.3	Electronic Nose systems	51
3.6.4	Quality determination of Orthodox Tea by E-nose systems	53
CHAPTER 4	MATERIALS AND METHOD	56
4.1	Steps for fabrication of ZnO based devices	56
4.1.1	Fabrication of ZnO Nanorods	56
4.1.2	Doping of ZnO	58
4.2	Fabrication of Dye Sensitized Solar Cells	60
4.2.1	Steps for fabrication	60
4.2.2	Dye deposition	60
4.2.3	DSSC assembling	61
4.2.4	Apparatus setup	61
4.3	Gas Sensors Measurements	62
4.4	Sensor Array and its Responses in Tea Infusion Vapour	63

4.5 E-Nose measurements	63
4.6 Correlating sensor signals with Tea-tasters scores	64
CHAPTER 5 RESULTS AND DISCUSSION	65
5.1 ZnO and its characteristics	65
5.1.1 X-ray Diffraction Analysis	65
5.1.2 Effect of Dopant Concentration	66
5.2 Dye Sensitized Solar Cell	69
5.2.1 Structure Characterization	69
5.2.2 Characteristics of Dye-Sensitized solar cells	71
5.2.3 The Equivalent Circuit Model of DSSC	72
5.2.4 Characterization of Dyes	73
5.2.5 Performance of the DSSC	74
5.2.6 Photovoltaic Properties	75
5.3 Gas Sensor	76
5.3.1 Response characteristics	76
5.3.2 Response sensitivity with operating temperature	78
5.3.3 Measurement of sensor characteristics	79
5.3.4 Doped ZnO materials for four different sensors	80
5.3.5 E-nose application of doped ZnO sensors for tea quality estimation	81
5.3.6 Principal component analysis	82
5.3.7 Development of E-nose response function	83
Chapter 6 Summary and Conclusion	86
Chapter 7 Recommendation and Future Work	89
REFERENCES	91

LIST OF TABLES

Table 1-1	Some application areas of DSSCs under development in various countries	14
Table 3-1	Basic physical parameters of ZnO at room temperature	21
Table 3-2	Reactions mechanisms that describe the functioning of a DSSC	31
Table 3-3	Physical changes in the sensor active films and the sensor devices used to transduce them into electrical signals	52
Table 5-1	Properties of doped and undoped sensing elements	68
Table 5-2	Solar cell parameters of the three DSSCs	76
Table 5-3	Sensor Characteristics of ZnO VOC Sensor	79
Table 5-4	Covariant Matrix formed from responses of four different sensors and its Eigen values	82
Table 5-5	Gradient of each sensor calculated from individual response	84

LIST OF FIGURES

Figure 3-1	Mechanism of sensitization by metal oxide additive	24
Figure 3-2	Schematic view of a dye-sensitized solar cell device	28
Figure 3-3	Dynamics of different electron transfer processes taking place in photo conversion by a DSSC	30
Figure 3-4	An example of an IV curve with different key parameters and output power (J-V) plot	38
Figure 3-5	Energy level diagram of a DSSC under illumination at open circuit	45
Figure 3-6	Scheme of processes, which determine the incident photon-to-current efficiency of DSSC	47
Figure 4-1	Flow chart for preparation of ZnO nano layer	59
Figure 4-2	Keithley 2400 Multimeter connected with computer system for sensor measurements	62
Figure 4-3	Sample measurement system in static gas environment	62
Figure 4-4	Schematic diagram of circuit and device connection for sensor measurement	63
Figure 4-5	Sketch of the Electronic Nose system used for the study	64
Figure 5-1	(a) X-ray diffraction patterns of ZnO thin film and (b) EDX analysis of ZnO Sample	65

Figure 5-2	SEM images of un-doped and doped ZnO thin films with (a) Undoped ZnO (b) Fe doped ZnO (c) Co doped ZnO and (d) Ni doped ZnO	67
Figure 5-3	Scanning electron microscope (SEM) picture of ZnO nanorod used in DSSC	70
Figure 5-4	Working principle of DSSC with various dyes	71
Figure 5-5	Equivalent circuit diagram of DSSC	72
Figure 5-6	Absorption spectra of rose bengal, pomegranate and mixed dye	73
Figure 5-7	Current voltage curves of various dyes based DSSC	74
Figure 5-8	Response of the ZnO nanowire gas sensors	77
Figure 5-9	Orthodox tea and CTC with varying temperature	78
Figure 5-10	PCA results of training data obtained from sensor array	82
Figure 5-11	Calculating of individual response gradient of four different sensor elements	83
Figure 5-12	Calibration of the sensors using a function built from individual sensor responses for Orthodox black tea	84

ABBREVIATIONS

AM	Air Mass
APCE	Absorbed Photon to Current (Conversion) Efficiency
DEP	Dielectrophoresis
DSSCs	Dye-Synthesized Solar Cells
E-Nose	Electronic Nose
EQE	External Quantum Efficiency
FE	Fermi Energy
FF	Fill Factor
HOMO	Highest Occupied Molecular Orbital
HTM	Hole Transport Material
IDE	Inter-digitized Electrode
IMPP	Current at The Maximum Power Point
IPCE	Incident Photon to Current (Conversion) Efficiency
IQE	Internal Quantum Efficiency
ITO	Indium-Doped Tin Oxide
LHS	Light-harvesting System
LCA	Life Cycle Cost
LUMO	Lowest Unoccupied Molecular Orbital
M_{pp}	Maximum Power Point
PES	Photoelectron Spectroscopy
PV	Photovoltaic
R_s	Series Resistance
R_{sh}	Shunt Resistance
SEM	Scanning Electron Microscope
SPD	Spray Pyrolysis Deposition
TBA	Tetrabutylammonium
TiO ₂	Titanium Oxide
UHV	Ultrahigh Vacuum
V_{MPP}	Voltage at The Maximum Power Point
V_{OC}	Open Circuit Voltage
XRD	X-Ray Diffraction
ZnO	Zinc Oxide

CHAPTER 1

1. INTRODUCTION

1.1. Nanotechnology and Nano devices

Nanotechnology is the application of nanoscience leading to the use of new nanomaterials and nanosize components in useful products. Nanotechnology will eventually provide us with the ability to design custom made materials and products with new enhanced properties, new nanoelectronics components, new types of solar cells and sensors, and even interfaces between electronics and physical systems [1].

In 1959, Nobel award winner Physicist Richard Feynman (father of nanotechnology) first proposed the seminal idea of nanotechnology by suggesting the development of molecular machines [1]. Ever since, the scientific community has investigated the role that nanotechnology can play in every aspect of society. The intrigue of nanotechnology comes from the ability to control material properties by assembling such materials at the nanoscale. The tunable material properties that nanotechnology can provide were stated in Norio Taniguchi's paper in 1974 where the term “nanotechnology” was first used in a scientific publication [2-3]. Nanotechnology has achieved tremendous progress in the past several decades. Recently, nanomaterials, which are materials with basic structural units, grains, particles, fibers or other constituent components smaller than 100 nm in at least one dimension [4], have evoked a great amount of attention for improving conversion efficiency of solar cells and other applications like, disease prevention, diagnosis, and treatment.

Nanomaterials include nanoparticles, nanoclusters, nanocrystals, nanotubes, nanofibers, nanowires, nanorods, nanofilms, etc. To date, numerous top-down and bottom-up nanofabrication technologies (such as electro-spinning, phase separation, self-assembly processes, thin film deposition, chemical vapor

deposition, chemical etching, nano imprinting, photolithography, and electron beam or nanosphere lithographies) [5] are available to synthesize nanomaterials with ordered or random nanotopographies. Nanomaterials can also be grown or self-assembled into nanotubes/nanofibers which can even more accurately simulate the dimensions of natural entities, such as collagen fibers. After decreasing material size into the nanoscale, dramatically increased surface area, surface roughness and surface area to volume ratios can be created to lead to superior physiochemical properties (i.e., mechanical, electrical, optical, catalytic, magnetic properties, etc.) [6]. Therefore, nanomaterials with such excellent properties have been extensively investigated in a wide range of applications, such as, medicine, electronic devices, solar cells and in particular sensor devices.

In the broadest sense, nanodevices are the critical enablers that will allow mankind to exploit the ultimate technological capabilities of electronic, magnetic, mechanical, and biological systems. While the best examples of nanodevices at present are clearly associated with the information technology industry, the potential for such devices is much broader. Nanodevices will ultimately have an enormous impact on our ability to enhance energy conversion, control pollution, produce food, and improve human health and longevity.

In this investigation, ZnO nanorods have been synthesized by sol-gel technique and few electronic devices have been designed and fabricated followed by details application study of these device elements.

The first application of fabricated nanorods in this investigation is Dye-sensitized solar cells (DSSCs). These are third generation solar cells. It lies in a category of photovoltaic device based on a photoelectrochemical system in which a porous oxide film with dye molecules adsorbed on the surface serves as the working electrode for light harvesting and the generation of photoexcited electrons [7-8]. The photogenerated electrons transfer from the dye molecules to the oxide, followed by diffusion in the oxide film and finally

they reach a transparent film that conducts the electrons to an external circuit. The oxidized dye molecules resulting from photoexcitation get reduced by receiving electrons from an electrolyte. The electrolyte is consequently regenerated through a neutralization of the positive ions with the electrons coming from the counter electrode, which is a platinum, carbon film coated on a glass substrate connected to the external circuit. In such a photoelectrochemical system, the dye molecules are designed to be highly sensitive to visible light so they are able to play a role in catching the incident photons effectively [9-10]. A variety of dyes have been intensively studied over the past two decades with attention being paid to increasing the molar extinction coefficient and/or extending the absorption range into the longer wavelength area [11]. Ruthenium complexes especially receive the most success in this regard and have become commercially available, known as N3, N719, and 'black dye', etc., [12]. On the other hand, the porous oxide film that acts as the backbone of the photoanode to carry the dye molecules has always been another one of the top concerns in the field of DSSCs. At this point, the flourishing development of nanotechnology opens a door to tailoring the materials with various nanostructures. When used in DSSCs, these nanostructures may provide a large surface area for dye adsorption and, moreover, make a difference to the behaviors of solar cells through affecting factors, such as the light propagation, electron transport, electrolyte (or I_3^- ions in electrolyte) diffusion within the photoelectrode film and so on.

The use of natural dyes in solar cells offers promising prospects for the advancement of this technology, because fabrication of cost effective solar cells is a scientific challenge. The use of natural pigments cut down the cost of chemical synthesis and high cost of rare metals need for metal organic dye sensitizers. Therefore, lot of interest has been drawn on natural dyes which extracted from plant materials. Several natural pigments have been utilized as sensitizers in photovoltaic cells due to their capability of injecting electron from excited pigments to the conduction band of the semiconductor material.

Most natural pigments that can be utilized in dye sensitized solar cells undergo rapid photo degradation. Rose Bengal, Pomegranate, Jamun (Indian Blackberry), Seabuckthorn are organic natural dyes of the anthocyanin and xanthene class found in leaves and fruits of plants and responsible for the colours of various vegetable tissues, which have been studied as a sensitizer in solar cells that are found to be photo stable.

The second application of fabricated nanorods in this investigation is Sensors for detection of volatile organic component in food, especially for detection of flavor in orthodox Darjeeling tea. For detection of organic flavor, a special technology called electronic nose was adopted. Electronic nose is a sensing technology where an array of sensors are used for simultaneously detect the signal and analyze them to find the contribution of individual component through sophisticated analysis techniques.

The present thesis has been arranged in the following sequence; Chapter 1 Introduction, Chapter 2 objectives in this thesis. Chapter 3 describes literature review, Chapter 4 presents the materials and method, Chapter 5 presents the results and discussion and finally, the thesis is concluded in Chapter 6.

1.2 Dye Sensitized Solar Cells

1.2.1 Problems in fossil fuels need for alternative source

If oil production remains constant until it's gone, there is enough to last 42 years. Oil wells produce less as they become depleted which will make it impossible to keep production constant. Similarly, there is enough natural gas to last 61 years and there is enough coal to last 133 years [13]. Nearly everyone realizes oil and gas will become scarce and expensive within the life times of living humans. An electricity shortage is felt by the most who depend on electricity for heating, cooking, and water supply. In these circumstances, a sustained energy crisis may become a humanitarian crisis. Inevitably, there will be a transition to sustainable energy sources. The transition may be

automatic or planned the choice is ours. If an energy shortage is prolonged a crisis management phase is enforced by authorities. Energy audits may be conducted to monitor usage.

In the worst kind of energy crisis energy rationing and fuel rationing may be incurred. Panic buying may beset outlets as awareness of shortages spread. Facilities close down to save on heating oil; and factories cut production and lay off workers. The risk of stagflation increases.

1.2.2 Harvesting solar energy

The Sun is the most plentiful energy source for the earth. All fossil fuel, hydro, wind, and biomass energy have their origins in sunlight. The Sun provides about 100000 TW to the Earth, which is approximately 10000 times greater than the world's present rate of energy consumption (13TW). Photovoltaic (PV) cells are being used increasingly to tap this huge resource of sustainable energy system and will play a key role in future. Our present needs could be met by covering 0.1% of the Earth's surface with PV installations that achieve a conversion efficiency of 10%.

The ever-growing energy demand and environmental impacts related to extensive exploitation of fossil fuels has motivated the search for alternative sources of energy. Development of new technologies allowing for the utilization of so-called renewable energy sources is under special attention. Renewable energy is derived from natural processes that are replenished constantly. So, from both economic and ecological point of view, tapping into these energy sources is desirable. The development of new technologies for power generation and optimization of the existing processes are, therefore, a matter of scientific, technological, economic and public concern. Therefore, the renewable share of worldwide electricity generation is expected to grow from 18 percent in 2007 to 23 percent in 2035 [13].

Power generation from solar photovoltaic (PV) cells has accelerated in the recent years. Apart from the increasing public awareness that the Earth's oil

reserves will run out in not so distant future, the development of photovoltaic technology is also promoted by an environmental concern among the society. In this respect, solar power generation comprises a promising electric power generation technology due to relatively low life cycle emissions of global warming gases. Concerned about climate change and energy dependence, governments introduced incentives to promote the adoption of solar energy and to shift consumption away from fossil fuels to a more secure supply. Because of these incentives, the photovoltaic industry grew in the last decade at a rate exceeding 30% per year [13]. An example of the booming of the photovoltaic market can be found in Europe. The energy system in Europe depends strongly on importations with about 80% of the energy consumption deriving from imported sources [14]. At the same time, Spain and other countries possess the most important solar resources in Europe (1200-1800 kWh.m⁻²year⁻¹) [15-16]. Although remarkable, this explosive growth was only possible because of the heavily subsidized program implemented by the European government. After this record-breaking year in 2008, the European government placed a cap limiting the number of new PV installations, because it was not possible to support the incentive program economically. As a consequence of this fact, together with the financial crisis, the number of new photovoltaic installations plumed dramatically to only 69 MW in 2009 [17]. The main problem in this context is the currently too high cost of energy generated by PV modules. There is still a long way to go in order to make the cost of photovoltaic energy generation comparable to that of electricity generated by power plants based on fossil fuels.

1.2.3 Solar Photovoltaic Cells

A solar photovoltaic cell is a semiconductor device that converts the energy of sunlight into electric energy. There are different types of solar cells. Crystalline silicon modules based on bulk wafers (including both large-grain polycrystalline and single-crystalline Si) dominate current production of Photovoltaic (PV) modules [18]. These devices are the main exponents of a

group named as the first generation of photovoltaic cells and they comprised about 85% of the market in 2009 [19].

The p-n junction is the classical model of a conventional solar cell [20]. This junction is created by doping different regions of the same semiconductor with different impurities. In this way, an interface between p-type and n-type materials is obtained, which creates a built-in electric field because of the different chemical potentials that electrons and holes have across the interface. This intrinsic electric field favours charge separation when a photon of energy larger than the band-gap creates an electron-hole pair near the interface.

Binary II-IV and II-V semiconductors such as GaAs, GaAlAs, GaInAsP, InAs, InSb and InP also fall into this group. They are interesting solar cell materials because they have near-optimal band gaps. However, these materials are extremely expensive. They have been used mainly in space solar cells, where performance is more important than costs. In addition, they can find a place in concentrating systems where the active surface area of the cells can be reduced significantly and, therefore, expensive materials can be used. Si-based first-generation PV is a robust and proven PV technology, but its cost reduction potential seems to be limited. In addition, although there is still room for improvement, efficiencies of silicon solar cells are yet close to the theoretical Shockley-Queisser limit for a single junction cell [18]. Two different approaches have been made to face the problems associated with first-generation PV: (a) to work on reducing the costs and (b) to increase the energy conversion efficiency beyond the Shockley-Queisser limit. The major thrust along the first approach is in developing thin film solar cells. These devices are usually referred to as second-generation PV. On the other hand, approaches focused on devices, which could theoretically overcome the Shockley-Queisser limit, form the basis of third-generation PV technologies.

Usually, wide band gap semiconductors as TiO_2 and ZnO are used as electron conductors and CuSCN as hole conductor. A wide variety of inorganic

absorbers [21] can be employed and the best efficiencies (3.5-4%) up to now for inorganic Extremely Thin Absorber (ETA) cells have been obtained using In_2S_3 [22]. In hybrid solar cells, in contrast to the previous two kinds of cells, both organic and inorganic materials are combined. They are usually composed of a conjugated polymer, which absorbs light and transports holes, and an inorganic electron conductor, both assembled together in a heterojunction. Power conversion efficiencies above 5% have been achieved with this type of cells [23].

It is still not clear, which one of all the technologies described above will determine the future of photovoltaics. Most probably, the optimum solution will depend on the respective application and on other factors as, for example, the location. In that case, a major diversification of the photovoltaic market will be the most likely scenario in the near future.

1.2.4 State of the Art in Solar Cells

Solar cells are usually divided into three main generations. The first generation contains crystalline silicon based solar cells that are relatively expensive to produce. Generally silicon based solar cells are more efficient and longer lasting than non silicon based cells. However, they are more at risk to lose some of their efficiency at higher temperatures (hot sunny days), than thin-film solar cells. Relative to the other types of cells, they have a higher efficiency up to 24.2%. The second-generation of solar cells is based on thin film technology and on a single junction and therefore share the theoretical efficiency limit with first-generation. Thin film devices comprise a smaller but rapidly growing segment of the PV activity. In the year 2009, the market share of thin film solar cells reached 15% [18]. The driving force for the development of thin film solar cells has been their potential for the reduction in manufacturing costs. The most efficient examples are solar cells made up of cadmium telluride (CdTe) and copper indium gallium diselenide (CIGS). Only

a thin film (of about 10 μ m thickness) is required for complete light absorption [24] as these materials are direct semiconductors. CdTe, for example, has a direct optical band gap of 1.5 eV that lies near the optimum band gap according to Shockley and Queisser [18]. In addition, thin film semiconductor materials can be deposited onto large surfaces, which is beneficial for volume production. PV modules based on crystalline silicon, in contrast, have to be assembled from individual cells. The efficiencies of second-generation devices, however, are typically lower than efficiencies of first generation cells. In contrast to PV devices based on Si wafers, which are already very close to the theoretical efficiency limit, thin film solar cells are still well below their potential. Thin film technologies are in the early manufacturing phase, and efficiencies of small-area laboratory devices do not easily translate into efficiencies of large modules. The highest performance obtained among all thin film technologies was for a CIGS cell of 1 cm² with 19.4 % [25]. The main issues associated with this kind of technology are the use of toxic materials as, e.g., cadmium and rare elements as telluride and indium. The implementation of a technology marketed as environmentally friendly that uses hazardous metals is quite controversial.

The third generation is used about solar cells that are very efficient and environmental friendly with low cost. Most technologies in this generation is not yet commercial, but there is a lot of research going on in this area. The goal is to make third generation solar cells cheap to produce.

The most well known studied unconventional photovoltaic system is the dye sensitized nanostructured solar cell developed by Professor M. Grätzel in 1991. At the moment this unique photoelectrochemical solar cell based on a TiO₂ nanoparticle photoelectrode sensitized with a light-harvesting metallo-organic dye, is on the verge of commercialization offering an interesting alternative for the existing silicon based solar cells as well as for the thin film

solar cells. At the same time the research activity as well as the industrial interest around the technology is growing fast.

The industry is starting to pay attention to this new technology and more than one hundred industrial laboratories worldwide are working on the development of DSSC-based photovoltaic devices [26]. DSSC technology possesses some clear advantages with respect to other photovoltaic devices. The first and probably the most attractive one for a practical application is its price. The technology shares the cost advantage of all thin film devices with respect to conventional photovoltaic technology. But, in contrast, it uses non-toxic materials and avoids costly production steps (e.g. high vacuum, high temperature, clean-room demands). However, there are still some bottlenecks in potential fabrication costs such as the price of the transparent conducting oxides used as substrate and of the dyes based on precious metals. Efficiency of the new DSSC technology must be above a certain threshold in order to compete with technologies already established. Although record efficiencies above 11% have been reached in the laboratory for small cell areas (typically in the sub-square-centimeter-range), these values reduce to around 8% during the scale-up of the area within a working module (25-100 cm²). In addition, a very controversial topic is the fact that after more than 20 years of research, the record efficiency is not much higher (11.1%) [27] than the one reported by Grätzel and O'Regan (7%) [28] in the Nature work, which opened the DSSC research field.

For the long-term industrial success of DSSC, its stability has been a big issue. For a 20-year lifetime of a device, its components must withstand several millions of turnovers. In addition, as any photovoltaic device, they have to stand very high temperatures, which can lead to structural transformation of the dye-TiO₂ system. Another crucial factor in the stability is the sealing. DSSCs (at least for the standard configurations) being liquid based devices, the sealing materials must avoid the evaporation of the

electrolyte as well as the accumulation of H₂O inside the cell. Moreover, the sealing material has to be chemically compatible with the solvent and components of the electrolyte.

Industrialization of DSSCs is in progress to overcome such issues and several successful tests of solar cells under outdoor conditions have been carried out. The stability of DSSCs was tested over 20,000 hours of simulated sunlight at an average light level corresponding to 0.8 sun¹ [26]. With respect to lifetime, the industrial DSSC company Dyesol reported accelerated aging tests, which indicated a service life of at least 27 years in the climate conditions of southern Europe. The substitution of organic solvents by non-volatile solvents is a very promising approach towards reaching such high stability demands. During the research work of this thesis, special attention has been paid to the stability of DSSCs and the use of non-volatile electrolytes (e.g. ionic-liquid-based) has been analyzed.

Another controversial issue concerning the industrialization of DSSC technology is the use of precious metals. Ruthenium, for example, is rather rare and the relatively small size of the market leads to highly volatile prices. However, the search for alternative dyes is a very active field and pure organic sensitizers have reached practically the same yield as ruthenium complexes [29]. Nevertheless, the contribution of ruthenium to the total price of the device is less than 0.01 €/pWatt [30] given the small amount employed. Nowadays the component of the DSSC that contributes most significantly to the final price of this technology is the transparent conducting oxide substrate (TCO). The most frequently used TCOs are fluorine- and indium-doped tin oxides. The price and availability of these TCOs significantly depend on the demand and the availability of Sn.

¹ One sun is equivalent to 100 mW cm⁻² illumination

Taking this into account, alternatives to Sn-based TCOs must be considered. DSSCs are compatible with various supporting materials as, for example, flexible ones. Apart from obvious advantages of flexible substrates in terms of versatility, they provide a mayor benefit to mass production: in contrast to glass, flexible substrates can be used in continuous roll-to-roll processes, making possible an extensive and low cost production.

Global climate change and air pollution problems are becoming serious and arousing public's concern on the emission of carbon dioxide and sulphur dioxide. The most representative aspect for environmental assessment is the weighting of emissions of these two gases. According to the ISO14040 standard, a life cycle assessment (LCA) was conducted to compare between a nanocrystalline DSSC electricity generation system and a natural gas/combined cycle power plant. The results show that the gas power plant generates emission at a rate of 450 g CO₂/kWh and the DSSC system only emits 19-47 g CO₂/kWh [33]. Most of the generation is due to the production process of the DSSC modules. The DSSC system was also compared with another thin film solar cell system made of amorphous silicon with emission rate of 42 g CO₂/kWh [33]. The studies indicate that DSSC has significant advantages and improvement in the increasing cell performance and energy conversion efficiency.

At this moment, DSSCs cannot compete with other photovoltaic technologies for grid connected solar farm applications. Photovoltaic devices in solar farms are designed to work under an optimal orientation and relatively strong light intensities. These working conditions are more suited for traditional PV. However, silicon panels suffer from significant loss of efficiency when working at low intensity levels or high temperatures [31]. In contrast, DSSCs perform particularly well under conditions corresponding to ~ 0.2 to 0.5 sun, and their efficiencies are practically independent of temperature in the range 25-65°C [30]. Over the same range of temperature, the efficiency of Si solar

cells diminishes approximately by 20% [30]. In addition, the efficiency of standard silicon technologies is much more dependent on the angle of incidence than in DSSCs. DSSCs perform well under diffuse light illumination or cloudy conditions and show high tolerance to partial shading. The combination of all the characteristics described above makes the integration of DSSCs into building architecture (an area known as Building Integrated Photovoltaic Applications, BIPV) one of the most interesting field of application for this new technology. First and second generation solar cells are only useful for roofs due to their high dependence on angle of incidence and direct light illumination. DSSCs are suitable also for some applications where the angle of incidence is far from optimal, as, for example, on facade [32]. DSSCs present also aesthetic advantages such as a wide range of available colors, non-reflectivity and partial optical transparency. The second main application for DSSCs is as alternative to batteries for stand-alone electronic equipment as, for example, mobile-phone chargers or decorative articles. An important property of this kind of products is their relatively short product life (up to five years, approximately). This makes possible a wider range of choice of materials due to the less demanding stability requirements. Flexible DSSCs are very suitable for this kind of applications, competing with flexible amorphous silicon. The key qualities of DSSCs are the customized colour options, wide variety of shapes, low light performance, excellent performance in diffuse light and a better average performance across the light range. Some of the application areas of DSSCs under development and the main companies working on this technology are summarized in Table 1.1.

DSSC technology is rapidly evolving toward full commercial viability. However, several issues have to be overcome before reaching a stage where it is ready to compete with other PV technologies.

Table 1-1 Some application areas of DSSCs under development in various countries [26]

Companies	Type of application
Sharp, Sony, Nanomax, IPP, FIS	Large area solar panels for terrestrial power generation
Dyesol - Italian BIPV Company, Color-Sol - project of Germany	Building Integrated Photovoltaic (BIPV)
Dyesol	Flexible power plastics
3G Solar of Israel	Power generation for remote area needs
SJC-Shimane Inst. of Industrial Tech.	Street lights and road signs
Sony's self-powering lamp shades	Consumer household electronics

Due to rapid escalation of prices of fossil fuels, there is a huge energy crisis all over the world and specially the developing and underdeveloped countries are affected for this. As a consequence, major thrust have been given by various countries for alternative source of energy. Nepal being situated in Himalayas, there was a possibility for oil exploration, but till date no such source have been explored. Moreover, Nepal is facing tremendous energy crisis, which is established by even sixteen hours of power cut per day during the dry season. This necessitates introduction of non-conventional energy sources urgently. However, the material cost for the components of solar cells is quite high. Alternative sources of energy with low component cost and ease of implementation is thus a matter to be focussed immediately. Dye Sensitized Solar Cells with natural dye are thus one of the most promising alternatives to cope with this energy crisis due to its ease of fabrication and easy availability of raw materials for fabrication.

To test the performance of DSSC, a small scale cell is usually used in the laboratory by proper internal and external device designs. The geometry of the test cells within a few square centimeters scale would affect the measured values of the photovoltaic properties of the cells. A mask is suggested to prevent the lateral light ray reflecting by the conducting glass. Grätzel's research group recently conducted a study on the effect of the mask aperture size contributing to the performance of the cell based on the photocurrent, photovoltage, fill factor and efficiency of DSSC [34]. Overestimation of the cell performance will be obtained if the cell is not covered with a designed mask. The thickness of the glass substrate can significantly affects the photocurrent density. In scaling-up the DSSC system into a 5cm x 5cm device, 5.52% conversion efficiency is achieved comparable to 6.16% for small-scale cell [35]. Shadow mask is applied in the large-scale DSSC to prevent overestimation and different light reflective backgrounds are tested. Further optimization on the photocurrent-photovoltage measurements of DSSC is required to achieve better and precise measured values for the experimental purpose and technological development.

1.3 Sensor Materials

1.3.1 Challenges in Sensors

Detection of aroma in food products is one of the major challenges today. A number of laboratories all over the world are working on detection of volatile organic components (VOC) that produces aroma in food products. As a consequence, technology commonly referred to as E-nose have been evolved. However, selectivity of sensor elements is one of the major issues which restrict the accuracy of detection procedure. To overcome this, various researchers adopted a number of statistical techniques like linear multiple regression, principal component analysis (PCA) and repetitive learning processes as back propagated Artificial intelligence etc. However, major

attention has to be given to design new sensing elements to improve the selectivity in the sensors.

Aroma is one of the most important sensory attributes of tea liquor. Tea flavor is particularly sensitive to compositional alterations of VOCs. The volatile compounds that contribute to tea flavor are produced through metabolic pathways during ripening, harvest, post-harvest and storage.

Tea quality indices could be correlated with electronic nose signal. Electronic nose (E-nose) was used to classify the tea into different mature groups rapidly and non-destructively, few literatures refer to establish a model using signal of electronic nose to predict the quality of tea.

1.3.2 State of the Art in Sensing materials

E-nose system is a sensor-based technology, which has the total headspace volatiles and creates a unique smell print. E-nose does not resolve the sample's volatiles into its individual components, but responds to the whole set of volatiles in a unique digital pattern. These patterns are signatures of the particular set of aromatic compounds. For each process or application of interest, a database of such digitized patterns is created, called the training set. When an unknown sample is exposed to the E-nose sensors, the E-nose first digitizes the sample's volatiles, and then compares it with the existing training set.

In the last decade, the electronic nose technology has opened the possibility to exploit, from a practical point of view, the information contained in the headspace in many different application fields. The E-nose offers a fast and non-destructive alternative to sense aroma, and, hence, may be advantageously used to predict the optimal harvest date. Commercially available electronic noses use an array of sensors combined with pattern recognition software. There have been several reports on electronic sensing in

the food industry [36]. Authors reported positive applications of electronic nose technology to the discrimination of fruits of different quality or ripeness, such as: oranges [37]; tomatoes [38]; apples [39-41], grain [42], but still few literatures are referred to monitoring of fruit shelf life and quality attribute [43]. The objectives of this study were: (1) to monitor flavour in orthodox Darjeeling tea using fabricated E-nose sensor and analyze the response use PCA; (2) to correlate the analyzed response with standard tea testers' scores to generate a calibration systems for prediction of quality of unknown tea sample.

CHAPTER 2

OBJECTIVES

Advanced materials are a topic of research for past few decades when a variety of devices was discovered. These devices include advanced sensors and energy conversion devices. Nanotechnology is another area of interest as it shows many new characteristics, which are unexplored earlier. One very interesting material in this regard is nanostructured ZnO [2-3]. They are easy to fabricate and possesses very interesting properties, which can be exploited to fabricate novel devices.

Owing to the problems discussed in the previous section, it is clear that, in order to overcome the high power consumption of the conventional energy conversion devices and their overheads, there exists a huge demand of low-cost PV cells with reasonable performance in terms of efficiency. Unlike the conventional, solid semiconductor solar cells (1st and 2nd generation), DSSC is a photo-electrochemical device whose operating principle mimics the photosynthesis reaction of the green plants [34]. The advantages of this technology lie in its simple and energy-efficient manufacturing, low cost, non-toxic and recyclable materials, and suitability for wide variety of end-user products, from small-scale power production to consumer goods. In this context, the research work conducted for this thesis was guided by the purpose of developing such cells using ZnO nanostructure based DSSC technology that uses locally available natural dye. In order to do so, it is very crucial to identify the advantages and limitations of ZnO as electron conductor in DSSCs.

The ZnO nanolayer properties varies with various kinds of dopant i.e., Fe., Co., and Ni. Aroma is one of the critical aspects of tea quality which can determine acceptance or rejection of a tea before it is tasted. Electronic noses

use an array of sensors combined with pattern recognition software. The doped ZnO was used as an array of sensors to form a e-nose capable of detecting volatile organic component in Tea flavour, which, in turn, analyses the flavour quality of tea.

The following specific objectives were identified and each of them has been achieved by trying to address several research problems under different sets of experiments:

- ❖ to identify an organic natural dye sensitizer suitable for ZnO,
- ❖ to investigate the electrochemical phenomenon and light energy conversion properties of ZnO nanostructure based DSSCs,
- ❖ to examine the influence of the semiconductor morphology on the performance of ZnO-based sensing elements,
- ❖ to test ZnO nanorods as sensing element for flavour in orthodox black tea infusion, and
- ❖ to use ZnO doped with different transitional elements as an array of sensors to form an e-nose capable of detecting volatile organic component in tea flavour, which, in turn, analyses the flavour quality of tea.

CHAPTER 3

3. LITERATURE REVIEW

3.1 Nano devices and Nanostructured sensing elements

Due to their unique properties, engineered nanoparticles are now used for a myriad of novel applications with great economic and technological importance. However, some of these properties, especially their surface reactivity, have raised health concerns, which have prompted scientists, regulators, and industry to seek consensus protocols for the safe production and use of the different forms of nanoparticles. However this large surface area also results in great benefits in important applications, like in photoanode in DSSCs [44]. Also sensitivity and selectivity of sensors can be affected by these nanomaterials [45].

3.2 ZnO Nanorods

3.2.1 The ZnO nanorods and its properties

Zinc oxide (ZnO) has been featured as subject of thousands of research papers, dating back as early as 1935 [46]. Valued for its ultraviolet absorbance, wide chemistry, piezoelectricity and luminescence at high temperatures, ZnO has penetrated deep into industries, and is one of the critical building blocks in today's modern society [47]. ZnO has been used as pigment, protective coating on metal surfaces and also in cosmetics as UV protection in sun creams because of its UV-absorbing characteristic. It has been employed in photodetectors, in particular in visible-blind UV detectors. ZnO nanostructures have been widely used for sensing applications because of their high sensitivity to the chemical environment. Other applications are in light emitting diodes and lasing. In recent years, a great interest has been paid to this oxide in the field of DSSCs.

There are few basic physical parameters for the ZnO at the room temperature which is listed in Table 3-1 [48-51]. There is still some uncertainty in the values of the thermal conductivity due to the presence of some crystal defects in the material [52]. In addition, a stable and reproducible p-type doping in ZnO is still a challenge and cannot be achieved. The findings regarding the values related to the mobility of hole and its effective mass are still arguable. The values of the carrier mobility can surely be enhanced after achieving good control on the defects in the material [53].

Table 3-1 Basic physical parameters of ZnO at room temperature [48-51]

S. No.	Parameters	Values
1	Lattice constants at 300 K	a = 0.32495 nm, c = 0.52069 nm
2	Density	5.67526 g/cm ³
3	Molecular mass	81.389 g/mol
4	Melting point	2250 K
5	Electron effective mass	0.28 m ₀
6	Hole effective mass	0.59 m ₀
7	Static dielectric constant	8.656
8	Refractive index	2.008, 2.029
9	Bandgap energy at 300 K	3.37 eV
10	Exciton binding energy	60 meV
11	Thermal conductivity	0.6 – 1.16 W/Km
12	Specific heat	0.125 cal/g°C
13	Thermal constant at 573K	1200 mV/K
14	Electron mobility	~210 cm ² /Vs

ZnO is a direct wide band gap (3.3 eV) [54] semiconductor with a large and diverse application potential. It crystallizes in three polymorphs: wurtzite, zinc blende and rocksalt structure. At ambient conditions, the thermodynamically stable phase is wurtzite, a hexagonal structure where each anion is surrounded by four cations at the corners of a tetrahedron and vice versa. The relatively open structure of zinc oxide allows plenty of sites to accommodate intrinsic defects and extrinsic dopants [55]. ZnO with a wurtzite structure is naturally an n-type semiconductor. It can be intrinsically doped via oxygen vacancies and/or zinc interstitials [56-57]. Extrinsicly, ZnO can be doped with both, n

and p-types [58]. A wide range of properties of this material depends on doping, including a range of conductivity from metallic to insulating, piezoelectricity, room-temperature ferromagnetism and chemical-sensing effects. The point of zero charge (pzc) of ZnO is observed at pH8 - pH9, depending on the preparation method and experimental conditions [56]. ZnO has a relatively poor chemical stability and is easily etched in acids and alkalis. Thanks to this relatively poor chemical stability, ZnO has probably the richest variety of nanostructures based on a very wide range of synthesis routes. Their morphologies include highly ordered nanowire arrays, tower-like structures, nanorods, nanobelts, nanosprings, nanocombs and nanorings among others.

Under general conditions, ZnO is single crystalline and exhibits a hexagonal wurtzite structure. The structure of ZnO nanorods could be revealed by X-ray diffraction (XRD) and scanning electron microscopy (SEM). Figure 5-1 shows the XRD pattern of the ZnO nanowire growth on an ITO coated glass substrate by using the spin coating sol-gel method. A dominant diffraction peak for (002) indicates a high degree of orientation with the c-axis vertical to the substrate surface. Figure 5-3 shows a top down image of ZnO nanorods. Both XRD and SEM demonstrate the hexagonal wurtzite structure of the ZnO nanorods.

3.2.2 Doping of nanostructured ZnO

Metal oxide semiconductor films have been widely studied and have received considerable attention in recent years due to their optical and electrical properties. Some of them are good candidates for transparent conductive oxide films. Among them, ZnO is one of the metal oxide semiconductors suitable for use in optoelectronic devices. It is an alternative material to tin oxide and indium tin oxide, which have been most used to date [59-60].

ZnO is an n-type wide band gap semiconductor (E_g 3.2 eV), and its electrical conductivity is due to intrinsic and extrinsic defects. The conductivity of pure

ZnO was produced by the former defects such as zinc excess at the interstitial position and the lack of oxidation. As pure ZnO thin films are sensitive to oxidation, absorption of O^{2-} in the films is inclined to decrease the electrical conductivity. In cases of doped ZnO with different dopants, the electrical properties are enhanced by extrinsic defects and these trials have been attempted [61-65]. Additionally, electrical properties of ZnO could be modified by thermal treatment in a reducing atmosphere [66]. The optical properties of ZnO were mainly affected by a surface morphology and the change of the optical energy band gap followed heavy doping [67]. The morphology was also modified by thermal treatment in a reducing atmosphere [68] and by an appropriate doping process [69].

Ohyama reported that the use of 2-methoxyethanol and monoethanolamine (MEA), solvents with high boil-ing point, resulted in transparent ZnO films with strongly preferred orientation [70] and that better electrical and optical properties had been obtained in 0.5 at.% aluminium doped ZnO thin films heated in reducing atmosphere [61]. Nunes found that when the doping concentrations of Al, In and Ga were 1, 1 and 2 at. %, respectively, electrical and optical properties of doped ZnO were superior [71].

ZnO thin films have been prepared by a variety of thin film deposition techniques, such as pulsed-laser deposition [72], RF magnetron sputtering [73], chemical vapor deposition [74], spray pyrolysis [75] and the sol-gel process [76]. While physical deposition such as pulsed-laser deposition and RF magnetron sputtering produce films with good electrical and optical properties at lower deposition temperature, it has disadvantages of a relative low deposition rate and a high cost for equipment. However, the sol-gel technique offers the greatest possibility of preparing a small as well as large-area coating of ZnO thin films at low cost for technological applications.

In this work, the effects of dopants and their doping concentration on the microstructure and electrical properties of doped ZnO thin films, as well as the interrelationship between the degree of crystal orientation and the

properties of films were investigated. The resistive response of the sensing element is supposed to vary with band gap energy of the substrate. Krylov [77] has found the following order of the activity variations: $\text{MnO}_2 > \text{CoO} > \text{Co}_3\text{O}_4 > \text{MnO} > \text{CdO} > \text{Ag}_2\text{O} > \text{CuO} > \text{NiO} > \text{SnO}_2 > \text{Cu}_2\text{O} > \text{Co}_2\text{O}_3 > \text{ZnO} > \text{TiO}_2 > \text{Fe}_2\text{O}_3 > \text{ZrO}_2 > \text{Cr}_2\text{O}_3 > \text{CeO}_2 > \text{V}_2\text{O}_5 > \text{HgO} > \text{WO}_3 > \text{ThO}_2 > \text{BeO} > \text{MgO} > \text{Al}_2\text{O}_3 > \text{SiO}_2$

As the potential between the sensor substrate and the gas molecule concerned, is dependent on electro negativity difference between them, variation in the band-gap energy of sensing substrate imparts larger cross-sensitivity between various species of gases to be determined. It was reported in [78] that blue and red shifts in band gaps observed for various transition metal ion-doped ZnO. So three transitional elements Fe, Co and Ni were selected from the reference [78], having largest variation in band gap energy.

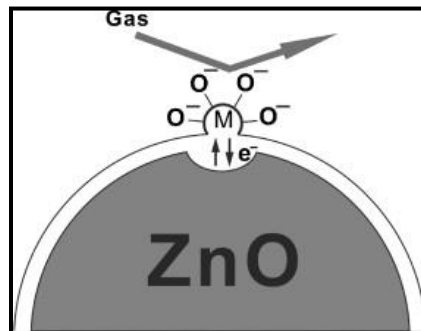


Figure 3-1 Mechanism of sensitization by metal oxide additive [79]

Recently, ZnO is alloyed with various “3d” transition metal (TM) ion for exploring its applicability in the field of gas sensors [78-79]. As shown in Figure 3-1, solutions were broken down into corresponding metal oxides during the heating process. The metal oxide particles adhered to the surface of pure ZnO widening the depletion layer, so the resistance of gas film increased. The resistance would decrease much more when test gas was in contact with the metal oxide particles for the wider depletion layer [39-40]. Thus, the response would be increased.

3.3 Dye Sensitized Solar Cells

3.3.1 Harvesting Solar Power: Solar Cells

Mankind has exploited solar power since ancient times, but it was not until the 19th century that a first approach to a photovoltaic use of solar energy was made. A French physicist, Edmund Becquerel [80], discovered the photovoltaic (PV) effect in 1839, when he observed that a voltage and a current were produced when a silver chloride electrode immersed in an electrolytic solution and connected to a counter metal electrode was illuminated with white light. Since that time, the idea of using the clean and abundant energy of the Sun and converting it into electricity has been a regular topic in the scientific community and in general to the society. However, it was not until the beginning of the 21st century that grid connected photovoltaic systems started to make a real contribution to electrical power generation. The birth of the modern era of PV solar cells occurred in 1954, when three Nobel laureates, D. Chapin, C. Fuller, and G. Pearson at Bell Labs demonstrated solar cells based on p-n junctions in single crystal Si with efficiencies of 5–6% [81]. From the mid 1950s to the early 1970s, PV research and development (R&D) was directed primarily toward space applications and satellite power. Then, in 1973, a greatly increased level of R&D on solar cells was initiated following the oil embargo in that year, which caused widespread concern regarding energy supply. Total global PV solar cell production increased from less than 10 MWp/yr in 1980 to about 1,200 MWp/yr in 2004 and the current total global PV installed capacity is about 117 GWp [82].

During the past decades several approaches to a third-generation of solar cells have been suggested. The term third-generation includes various technologies. Generally, this term is used to describe systems which do not fall into the first- or second-generation and/or which try to circumvent the 31% Shockley-Queisser limit [24]. Various approaches to achieve efficiencies above 30%

have been explored. Tandems of cells provide the best known example of how such high efficiency might be achieved. In this case, conversion efficiency can be increased by stacking cells of different band gaps thus increasing the spectral sensitivity [83]. In principle, by stacking a large number of suitably tailored and designed cells, efficiencies as high as 67% and 86% for un concentrated and maximally concentrated solar illumination are theoretically possible [18].

In the 1990s, new concepts of solar cells based on nanostructured and organic materials were conceived as a new approach to low-cost photovoltaics. The most active research fields comprise organic heterojunctions [84], extremely thin absorber (ETA) cells [21,85-86], hybrid solar cells [87-88] and dye-sensitized solar cells [28]. These new solar cells have a big potential of development since molecular and nanostructural engineering approaches can be exploited for further improvement. In an organic heterojunction the active layer is made up of two materials: a donor (n-type) and an acceptor (p-type). Poly-phenylene vinylene derivatives and poly-alkylthiophenes are common donors; fullerene and its derivatives are common acceptors. The best confirmed photo-conversion obtained for this type of devices is 5.15% [25]. The three-phase ETA cells are completely made up of solid inorganic materials. In these cells, a thin light absorbing semiconductor is sandwiched between two transparent, highly interpenetrated nano-structured semiconductors which act as electron and hole conductors [85,89-90].

As discussed in the previous sections, the widely accepted paradigm in traditional solar energy conversion is to use highly pure semiconductor materials (avoiding defects and interfaces) and to rely on a built-in electrical field to assist the separation of photo-generated electron-hole pairs. Besides, a semiconductor band gap close to an optimum for solar energy absorption is desirable. In this regard, dye-sensitized solar cells (DSSCs) marked a fundamental innovation as they rely on nano-structured, wide band gap

semiconductors. DSSCs work without the need for a built-in electrical field, without a strict control of the purity of materials.

Dye-sensitized solar cells (DSSCs), which are based on oxide semiconductors and organic dyes or metal organic complex dyes, are one of the most promising candidate systems to achieve efficient solar-energy because they are flexible, inexpensive, and easier to manufacture than silicon solar cells [91]. ZnO-based DSSC technology alternative to TiO₂ is considered as one of the most promising materials for solar cells due to a faster electron transport with reduced recombination loss and its ease of crystallization and anisotropic growth. Ko *et al.* [92] compared different fabricated ZnO nanowire DSSCs that included lengthwise growth (LG) and branched growth (BG). They showed that the overall light-conversion efficiency of the branched ZnO nanowire DSSCs was much higher than the upstanding ZnO nanowires. The reason for the improvement is the enhanced surface area for higher dye loading, light harvesting and the reduction of charge recombination by providing direct conduction pathways along the crystalline ZnO.

Lupan *et al.* [93] studied the well-aligned arrays of vertically oriented ZnO nanowires electrodeposited on ITO coated glass for dye-sensitized solar cells. The maximum overall photovoltaic conversion efficiency was 0.66% at 100 mW/cm². Cheng *et al.* [94] fabricated branched ZnO nanowires on conductive glass substrates via a solvothermal method for dye-sensitized solar cells. The short-circuit current density and the energy conversion efficiency of the branched ZnO nanowire DSSCs are 4.27 mA/cm² and 1.51%, which are higher than those of the bare ZnO nanowire. Sudhagar *et al.* [95] reported jacks-like ZnO nanorod architecture as a photoanode in dye-sensitized solar cells and the result exhibited a higher conversion efficiency of $\eta = 1.82\%$ ($V_{oc} = 0.59$ V, $J_{sc} = 5.52$ mA cm⁻²) than that of the branch-free ZnO nanorods electrodes ($\eta = 1.08\%$, $V_{oc} = 0.49$ V, $J_{sc} = 4.02$ mA cm⁻²).

DSSCs [28] are based on nanostructured wide band gap semiconductor films photosensitized with a dye. In 1991, Grätzel and O'Regan reported on a

device made of sensitized nanoporous TiO_2 with a conversion efficiency of 7.1% [28]. This discovery opened a new field of scientific research and since then many research groups have worked on the improvement of the efficiency and the stability of this kind of solar cells. This field has experienced a boom in the last decade, with two or three research articles published every day. At the time of writing, the conversion efficiency of DSSC using high haze TiO_2 electrodes has been reported to be 11.1% by the Solar Systems Development Center, Sharp Corporation, Japan, in 2006 [27].

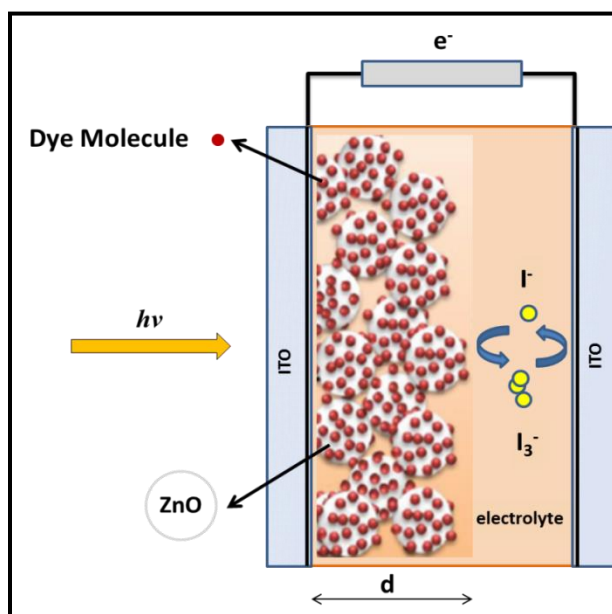


Figure 3-2 Schematic view of a dye-sensitized solar cell device

The backbone of a DSSC is a mesoporous layer of semiconductor oxide nanoparticles, which are sintered together to establish a good electric contact between the particles. The film thickness (d) is usually around $10\ \mu\text{m}$ and the nanoparticles are around $25\ \text{nm}$ in diameter. This film is deposited on a glass plate covered with a transparent conducting oxide (TCO), which allows light to enter in the cell. Attached to the surface of the oxide there is a monolayer of dye molecules, which are responsible for harvesting the light. The sensitized film is surrounded by an electrolyte solution of high ionic strength, usually composed of an organic solvent containing a redox pair.

Nearly all the components of a DSSC are tuneable. Up to now, the most successful combination of materials is still the one reported in the pioneering work by the Grätzel group [88], which opened the research field of dye-sensitized solar cells. In this configuration, the main components are a layer of zinc oxide nanoparticles sensitized by a natural dye with the I^-/I_3^- redox couple in an organic solvent, which acts as the redox mediator. Grätzel and O'Regan found a successful combination of a nanostructured semiconductor electrode with an efficient and stable dye. The key factor of that combination, as Tsubomura *et al.* [96] already pointed out for ZnO mesoporous electrodes in 1976, was the surface area. In a mesoporous film, the incoming photons can be captured efficiently although the surface is covered only by a monolayer of dye [97]. The reason is that a mesoporous structure can have a surface area available for dye adsorption more than a thousand times larger than a flat electrode of the same geometric area. The research work in this thesis is based on alternative materials to this standard configuration. The characteristic of each standard component as well as the advantages and disadvantages of alternative materials will be described in the following chapters.

An energy diagram of DSSCs as the one shown in the figure should not be taken as a real interpretation of the actual energetic situation in a DSSC. The indicated values may be taken from measurements of the individual components, excluding effects caused by the interaction among them [98] and potential energy (e.g. conduction band energy) and free energy (redox energy) scales are mixed [99].

3.4 Operational Principles of Dye-sensitized Solar Cells

DSSCs are photo electrochemical devices where several electron transfer processes run in parallel. In a DSSC, optical absorption and charge-generation are separate functions. The role of dye molecules is the same as that of

chlorophyll in leaves: they must absorb the incident sunlight and induce an electron transfer reaction. Dye-sensitized solar cells are photo regenerative devices, basic working principles of which are summarised in Table 3-2.

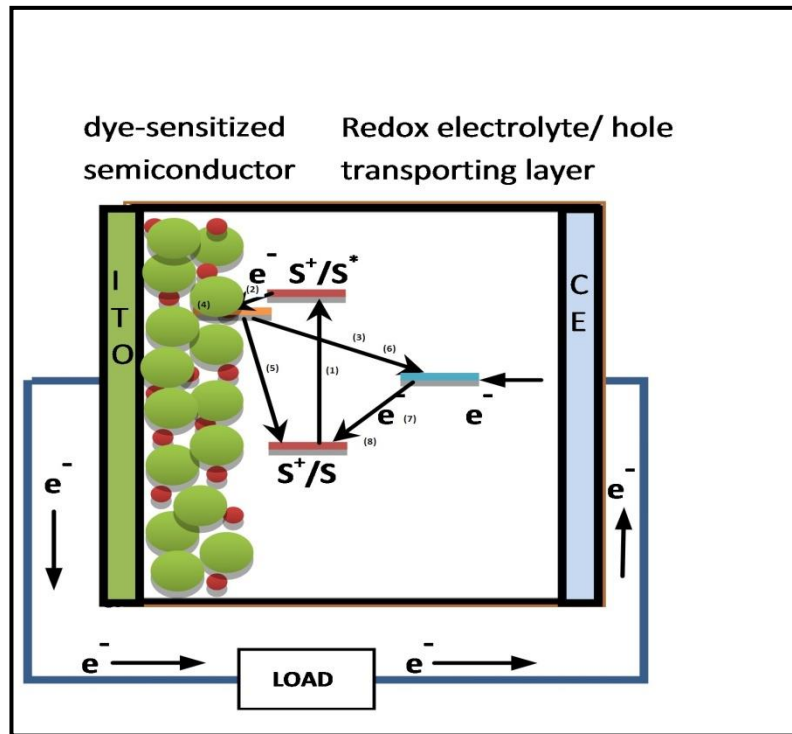


Figure 3-3 Dynamics of different electron transfer processes taking place in photo conversion by a DSSC.

Upon illumination, photoexcitation of the dye results in the injection of an electron into the conduction band of the oxide. The oxidized sensitizer thus formed can recombine with the injected electron or the electron donor in the electrolyte can regenerate it. Also relaxation of the excited dye before electron injection may occur. The photogenerated electron travels through the mesoporous oxide film by a random walk process [100-101] towards the external contact. The extracted electron can then perform work in an external circuit and return to the counter electrode. The oxidized species in the electrolyte produced upon the dye regeneration step diffuses to the carbon coated counter electrode, where it is reduced back, closing the regenerative cycle. The major loss channel in the process is the recombination of the

injected electrons with the oxidized redox mediator. The timescale of the different processes is the key point for obtaining high energy conversion efficiency of these devices, as will be discussed below.

Table 3-2 Reactions mechanisms that describe the functioning of a DSSC

1.	Photoexcitation	$S + h\nu \rightarrow S^*$
2.	Electron injection	$S^* \rightarrow e^-_{(CB)}(SC) + S^+$
3.	Relaxation	$S^* \rightarrow S + h\nu$
4.	Electron transport	$e^-_{(CB)}(SC) \rightarrow e^-(TCO)$
5.	Recombination with the dye	$S^+ + e^-_{(CB)}(SC) \rightarrow S$
6.	Recombination	$2 e^-_{(CB)}(SC) + I_3^- \rightarrow 3I^-$
7.	Dye regeneration	$2S^+ + 3I^- \rightarrow 2S + I_3^-$
8.	Reaction at the counter electrode	$I_3^- + 2e^-(C) \rightarrow 3I^-$

Symbols: S (fundamental state of the dye),
 S* (excited state of the dye),
 S⁺ (oxidized state of the dye),
 h (Planks constant)
 ν (Photon frequency)
 SC (semiconductor),
 CB (conduction band),
 TCO (transparent conducting oxide)

The maximum theoretical value for the photovoltage at open circuit condition is determined by the potential difference between the conduction band edge of the ZnO and the redox potential of I⁻/I³⁻ couple in the electrolyte.

There have been several theoretical calculations on the maximum power conversion obtainable for solar radiation using a single-junction (p-n) solar cell. The theoretical considerations of Shockley and Queisser establish an upper limit of the efficiency of 31% for a semiconductor with a band gap energy (E_g) of 1.3 eV under AM 1.5 illumination [102]. There are two main reasons for such a low maximum efficiency. On the one hand, photons with an energy E < E_g are not absorbed by the solar cell. On the other hand, even electrons excited by photons with an energy E > E_g can only deliver the band gap energy (E_g) to the electric circuit, whereas the rest (E-E_g) is lost by thermal dissipation [98]. Based on this theoretical maximum conversion

efficiency and on the nature of materials, photovoltaic cells can be grouped in three major categories or generations. The first group includes cells that use materials of high purity and containing low concentrations of structural defects. These are the most efficient cells up to date. To this group belong, as already mentioned, crystalline silicon solar cells with a confirmed record efficiency of 25% by the time of writing [103]. Although it has been the material, most frequently employed and studied, silicon is not an ideal semiconductor for photovoltaic conversion. Since it is an indirect semiconductor, its optical absorption coefficient is low. Therefore, Si wafers with a thickness of more than hundred microns are needed to efficiently absorb most of the incident light. This, together with costly purification and crystallization processes of silicon, make the production of silicon cells very expensive.

3.4.1 The dye: light harvesting and charge separation

The semiconductor oxides used in DSSCs are wide band gap materials, which do not absorb in the visible range. The function of harnessing the solar light is carried out by the sensitizer molecules attached to their surface. The absorption spectrum of the optimum dye for DSSCs should cover the whole visible region and even part of the near-infrared (ideally, a threshold of 920 nm should be harvested [26]). In addition, the dye must have suitable anchoring groups, which firmly attach the molecule to the semiconductor oxide. Upon light absorption, the dye molecule is promoted to its excited state (reaction 1, Table 3-2). From this excited state, the dye molecule can return to its ground state (reaction 3) or can inject an electron into the conduction band of the semiconductor (reaction 2). In order to understand the mechanism of charge separation in DSSCs, the time scale of processes 2 and needs be compared. The key rate requirement at this step is that injection must be at least 100 times faster than the relaxation of the dye from its excited state [104]. The kinetics depends on several factors, which are principally determined by the properties of dye and the semiconductor. In the case of

standard cells with ruthenium-complex dyes, the relaxation of the sensitizer is believed to occur at a rate that is several orders of magnitude slower ($\sim 10^{-8}$ s) than that of the forward injection ($\sim 10^{-13}$ s) [105]. The presence of a local electrostatic field is not required because the charge separation is achieved due to the large kinetic asymmetry between the forward electron transfer and the back relaxation.

In the injection dynamics of DSSCs, the energy difference between the conduction band of the semiconductor and the excited state of the sensitizer is a determining factor [49] and for successful sensitization, the dye LUMO level must be higher in energy than the conduction band of the semiconductor [99]. The driving force necessary for a rapid vectorial charge displacement is believed to be small (around 0.1 eV) for ruthenium-complex dyes. Generally, it is accepted that electron injection is very fast and, at least for ruthenium-based dyes and titanium dioxide, injection is not considered a limiting factor in the DSSC performance. However, recently Koops *et al.* [104] reported a slow injection time in the presence of tert-butylpyridine and Li^+ . These are common electrolyte additives that, as will be discussed in following chapters, are added to the device to improve cell performance. According to these authors, in some cases injection is slow enough for kinetic competition with relaxation of the dye.

Ruthenium-complex dyes are the most used as well as the most successful sensitizer in DSSCs. These dyes exhibit a strong absorption in the visible and a long-lived excited state (20-60 ns) [98] due to the metal-to-ligand charge transfer (MLCT) character of their light absorption [106]. In a molecule with a MLCT transition, the highest occupied molecular orbital HOMO is located near the metal while the lowest unoccupied molecular orbital LUMO is located near the molecule ligands. Upon illumination, electrons are promoted from the ruthenium metal center to the carboxylated bipyridil ligands. These carboxylate groups are directly coordinated to the surface titanium ions producing intimate electronic contact between the sensitizer and the

semiconductor [105]. The dye possesses directionality in the excited state and it is one of the reasons for the fast electron transfer process at the dye/TiO₂ interface. Among thousands of dyes explored in the last two decades, the best performing DSSC have been fabricated with ruthenium-complex dyes. Although this kind of complexes seem to be appropriate sensitizers for TiO₂, it has been proved that ruthenium dyes are not suitable for ZnO. To look for a more appropriate natural dye for this semiconductor has been one of the aims of this thesis.

3.4.2 The electrolyte: regeneration of the dye and hole conduction

The electrolyte is one of the key components in a DSSC, which plays different roles in the functioning of the device. The basic components of a standard electrolyte are a solvent and a redox couple. Besides, some additives are usually present in the electrolyte that are not essential for the functioning of the cell, but have been proved to lead to better cell performances. The most frequently used and at the same time the most successful electrolyte up to now in a DSSC is composed of the redox couple I⁻/I³⁻ in an organic solvent. Some other redox shuttles, for example cobalt-based systems [107], SCN⁻ / SCN³⁻ [108-109] and SeCN⁻/SeCN³⁻ [108-110] have also been explored but iodide-based electrolytes are found to be well suited for DSSCs and no other known redox couple works nearly as well [116].

After photo induced electron injection from the dye into the conduction band of the semiconductor, the dye is in its oxidized state and must be reduced by an electron donor in the electrolyte. The regeneration of the dye to its ground state must be faster than the recombination with conduction band electrons (reaction 5, Table 3-2). The concentration of iodide ions in the DSSC is usually very high ($>10^{20}$ cm⁻³ /0.5 M) and regeneration of the dye by the most common ruthenium-complex sensitizers is a very fast reaction ($\sim 10^{-6}$ – 10^{-9} s) [98, 111-113]. Rapid regeneration kinetics of the oxidized dye by iodide was also observed in organic sensitizers such as chlorophyll derivate [58] and a

porphyrin (ZnTPPC) [59]. Thus, recombination with the dye is usually neglected [60] as a loss mechanism in a DSSC.

The driving force that makes the regeneration of the dye possible is the difference in the oxidation potential of the dye and the electrolyte (Figure 3-3). A driving force ≥ 0.5 V has been measured for ruthenium-complex sensitizers and also for some organic dyes [114-115]. However, recently Wenger *et al.* [116] demonstrated that a metal-free organic sensitizer with a measured driving force for regeneration of only 0.150 V can operate functionally in DSSCs. This opens to the possibility of reducing photovoltage losses due to poor energetic alignment of the components and of using dyes with smaller band gaps that consequently absorb in the infrared. The detailed mechanism of the dye regeneration reaction has not been fully elucidated and numerous factors appear to influence its rate. Apart from the oxidation potential of the dye, this rate was found to depend strongly on the nature and concentration of the cations present in the electrolyte solution [111]. Pelet *et al.* also found that the nature of cation of the iodide salt has a significant effect on regeneration: rapid regeneration occurs in the presence of small cations capable of specifically adsorbing onto the TiO₂ surface, such as Li⁺ and Mg²⁺, whereas much slower regeneration was found with tetrabutylammonium, TBA⁺ ions. This effect was attributed to the resulting higher local iodide concentration near the TiO₂ surface when positive charge is adsorbed.

The photovoltage of the cell depends to a great extent on the redox couple, which sets the electrochemical potential at the counter electrode. The electrolyte also affects the electrochemical potential in the semiconductor oxide, as recombination of electrons with the oxidized species in the electrolyte is the main loss mechanism in the cell. In fact, the main quality of the iodide/triiodide couple is a much slower kinetics of recombination with electrons in the conduction band as compared to other redox couples.

Transport of the redox mediator between the electrodes is mainly driven by diffusion. Triiodide must migrate from the photoelectrode to the counter

electrode, where it is reduced to iodide. Simultaneously, the reduced iodide must diffuse to the vicinity of the oxidized dye molecules within the cell. These processes depend on mass transport of both species in the electrolyte. In typical electrolytes, sufficient excess of I⁻ is employed and its concentration is around ten times higher than that of tri-iodide. This higher concentration, in addition to a higher diffusion coefficient of I⁻ with respect to I³⁻, makes the current limitation mainly due to diffusion of the triiodide ions. Apart from diffusion coefficient and concentration of the species, another key factor in this diffusion process is the distance between the electrodes [117].

Different alternatives to the standard electrolyte described above have been explored as hole conductors for DSSCs. To overcome problems associated to evaporation of the organic solvents, they are often replaced by ionic liquids. Ionic liquids have a much higher viscosity than organic solvents, but they have a negligible vapour pressure which makes them free of evaporation problems. Other alternatives to the standard DSSC electrolyte are used in solid state devices in which the liquid electrolyte is replaced by a p-type semiconductor or a p-type organic material. The hole conductor needs an intimate contact with the dye monolayer covering the porous semiconductor to efficiently regenerate the dye. In standard DSSCs, this is easily achieved as the liquid electrolyte penetrates completely in the nanostructure. In contrast, inefficient pore filling, together with high recombination rates with conduction band electrons are the main limitations of solid-state devices. Spiro-MeOTAD is the most used p-type material [118-119].

3.4.3 The counter electrode: regeneration of the oxidized species in the electrolyte

After diffusion through the electrolyte, triiodide is reduced to iodide at the counter electrode. The counter electrode in a DSSC is usually formed by a thin catalytic layer of carbon onto a conducting glass substrate. An over potential is needed to drive this reaction at a certain current density. This exchange current density for the redox system should be as high as possible in

order to minimize the kinetic over potential. It has been shown that the over potential at the counter electrode is small, less than 20 mV [99], as the exchange current density at a platinum-coated electrode is sufficiently high at about 10-100 mAcm⁻² [105]. This is indicative of the excellent catalytic properties of platinum.

3.4.4 The mesoporous semiconductor: ZnO as electron conductor in DSSCs

The semiconductor oxide is the physical support of the sensitizer molecules and the electron conductor in a dye-sensitized solar cell. As mentioned before, the mesoporous structure of the films is crucial for a high dye loading in the semiconductor. The wide band gap semiconductor titanium dioxide (TiO₂) has been by far the most widely used DSSC photoelectrode material. TiO₂ is a very versatile, non-toxic, cheap and chemically stable material and its suitability for DSSCs has been extensively proved. Many other wide band gap oxide semiconductors have been also explored as potential electron conductors in DSSCs. However, till this date, no other material has reached efficiencies comparable to TiO₂. Nevertheless, some semiconductors present special characteristics that make them very attractive candidates as alternatives to TiO₂ and ZnO. The conduction band edge of SnO₂, for example, lies around 0.5 V lower than the one of TiO₂. SnO₂ can be used, therefore, in combination with dyes with absorption close to the infrared that are unable to sensitize TiO₂. The band gap and conduction band edge of ZnO are similar to that of anatase TiO₂ [120-121]. However, single-crystalline ZnO presents much higher electron mobility than anatase TiO₂, which should favour electron conduction TiO₂ [121-124].

3.5 Theoretical description of dye-sensitized solar cells

3.5.1 Current-voltage characteristics

A solar cell is a particular case of a diode, an electrical device, which favours current flow in one direction, but not in the opposite. A diode has a certain characteristic relationship between produced current and applied voltage. This relation is known as the current-voltage characteristics or IV curve of the diode and it is expressed as:

$$J = J(V) \quad 3-1$$

where, J is the DC electrical current density running through the device and V is the externally applied bias.

The universal shape of an IV curve in a solar cell (Figure 3-4) is a consequence of the balance of two opposing mechanisms: (1) light-induced charge separation and subsequent current generation and (2) loss processes (recombination).

The application of an external forward bias to the solar cell implies the accumulation of electrons within the anode. This leads to an increase of the dark current that opposes the current generated by the cell. The net current tends to cancel at sufficiently high bias (open circuit conditions). At zero bias the cell produces its maximum current (short circuit conditions). The solar cell generates power when it produces current at non-zero bias.

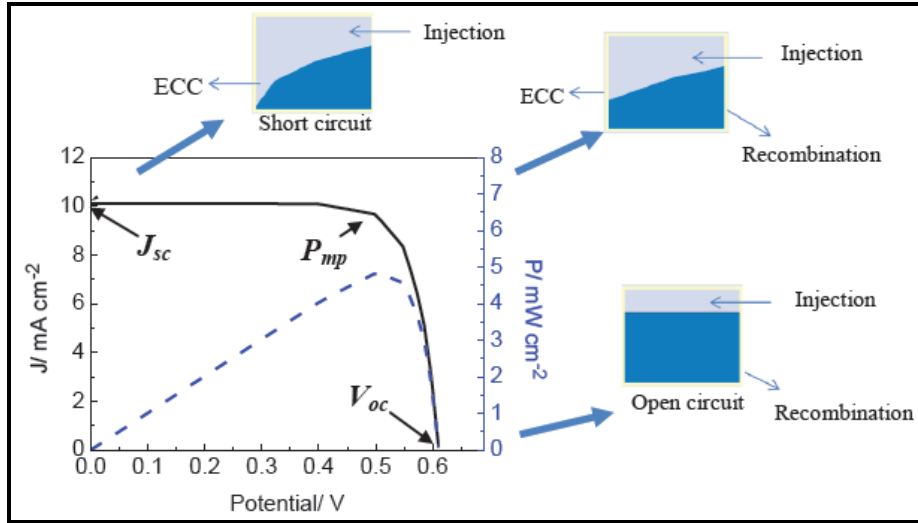


Figure 3-4 An example of an IV curve with different key parameters and output power plot [121].

Symbols: J_{sc} (short circuit current density),
 V_{oc} (open circuit voltage),
 P_{mp} (maximum power point),
ECC (external current collection)

From a practical point of view, the most important piece of information one can obtain from an IV curve is the maximum output power of the device per unit area, P_{mp} . The maximum power point in an IV characterization is defined by the square under the IV curve with the largest area, a point which yields the maximum product of current and voltage. Other important parameters in every IV curve are the current density at short circuit conditions (short circuit current density, J_{sc}) and the voltage at open circuit conditions (open circuit voltage, V_{oc}). The behaviour of a solar cell can be described, in its simplest form, by the diode equation. Assuming no series or shunt resistances, this can be written as [125]:

$$J = J_{sc} - J_0 \left(\exp\left(\frac{qV}{AkT}\right) - 1 \right) \quad 3-2$$

where, J_{sc} = short circuit photocurrent,
 J_0 = exchange-current,

q = elementary charge,
 k = Boltzmann constant,
 T = absolute temperature, and
 A = ideality factor.

The shape of an I - V curve is described by the fill factor (FF). The fill factor is a phenomenological quantity, with a value between 0 and 1, being close to one in the case of an ideal diode ($A = 1$) and related to the non ideality factor m . It defines the ratio of the actual maximum power ($V_{mp} \cdot J_{mp}$) to the maximum power theoretically attainable by the solar cell ($J_{sc} \cdot V_{oc}$). The overall solar-to-electrical energy conversion efficiency of a solar cell (η) can be expressed as

$$\eta = \frac{J_{sc} V_{oc}}{P_{in}} FF \quad 3-3$$

where P_{in} is the power density ($W\ m^{-2}$) of the incident light.

3.5.2 Electron recombination and the origin of the photovoltage in DSSCs

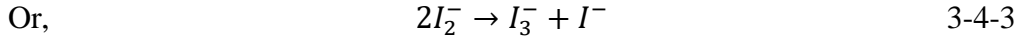
As already mentioned, the main loss process in a DSSC is the recombination of injected electrons in the conduction band of the semiconductor with oxidized species in electrolyte. The majority of theoretical and experimental studies about the recombination kinetics in DSSCs are based on the iodide/triiodide redox couple. It is generally accepted that the net recombination reaction between TiO_2 and this redox couple is a two electron reaction [126] given by



Two possible intermediate steps are possible for the reaction expressed above, a first elementary step consisting in electron capture by I_3^- to form iodine radical ion I_2^- .



followed by two possible second steps involving I_2^- .



Therefore, it is believed that the reaction is constituted of a multiple-step mechanism, very probably involving the species I_2^- with one of the steps being rate-determining. After more than one decade of research, the exact nature of this electron transfer is still not known in detail. It is believed to depend on specific factors of the device such as the dye molecule and the electrolyte solvent [127]. In any case the reaction has been shown to be approximately first order with respect to either of these iodide species, I_2^- or I_3^- [128].

According to classical chemical kinetics, the rate of back reaction (U) (measured in $\text{cm}^{-3}\text{s}^{-1}$) depends on the reactant concentrations and the rate constants for electron transfer

$$U = k_0 n^{v_e} [I_3^-]^{v_{I_3^-}} \quad 3-5$$

where, k_0 is the rate constant for the back reaction of electrons; n , the electron concentration and the exponents represent the reaction order with respect to electrons and tri-iodide ions, respectively. In order to make progress towards a simple model that describes the recombination process in DSSCs, several assumptions are made:

- The reaction is first order in both, electron and triiodide concentration
- Electrons can be transferred only from the conduction band (i.e., they are not trapped when recombining)
- Triiodide concentration is many orders of magnitude larger than the electron concentration in the oxide and can be treated as a constant

Assuming these statements, the equation above can be formulated as a first order reaction in terms of the free electron concentration:

$$U_n = k_r n_c \quad 3-6$$

where k_r corresponds to $k_r = k_0 [I_3^-]$ and n_c is the free electron concentration (concentration of electrons in the conduction band). This linear recombination term was introduced in the theoretical model proposed by Södergren *et al.* [129] in an early stage of DSSC research. However, it has been found that this model cannot describe DSSC characteristics quantitatively [130]. As will be shown several times in this thesis, this simple recombination term implies an ideal behaviour of the solar cell (an ideal diode). However, evidence for non-linearity in the recombination is often found in DSSCs, also for the ZnO solar cell studied here. For example, the measurement of the charge transfer resistance or recombination resistance in a DSSC is commonly affected by non-ideal features. To get insight into this point it is necessary to start from the definition of the recombination current which given by:

$$j_{rec} = qdU_n \quad 3-7$$

where, q is the elementary charge and the thickness of the film. From the reciprocal derivative of this recombination current with respect to voltage [131], the recombination or charge transfer resistance (R_{ct}) is obtained:

$$R_{ct} = \frac{1}{A} \left(\frac{\partial j_{rec}}{\partial V} \right)^{-1} \quad 3-8$$

where, A is the cell surface area. Combining the above two equations, the recombination resistance can be related to the derivative of the recombination rate:

$$R_{ct} = \frac{1}{qdA} \left(\frac{\partial U_n}{\partial V} \right)^{-1} \quad 3-9$$

Experimentally, it is found that the resistance fits to the following empirical equation when measured as a function of applied (forward) bias.

$$R_{ct} = R_{ct,0} \exp \left(-\beta \frac{qV}{kT} \right) \quad 3-10$$

where, $R_{ct,0}$ is a constant and β the so-called transfer parameter. In a linear (ideal) model, β would be equal to one. However, in experimental measurements of the charge transfer resistance for DSSCs usually a parameter $\beta < 1$ is observed [130]. This is interpreted as an indication of non-linear recombination in DSSCs. If we assume a non-linear recombination model, Equation 3-6 can be rewritten as:

$$U_n = k_r n_c \beta \quad 3-11$$

where β , the transfer coefficient, defines the recombination order in the sublinear recombination kinetics. Using Equations 3-9, 3-11 and the relation between the free electron concentration and the voltage that will be described below (Equation 3-18), the empirical expression of Equation 3-10 is obtained. Hence, the experimental transfer coefficient is shown to be equivalent, according to this description, to the electron reaction order in Equation 3-11. The origin of non-linearity or non-ideality (we have just shown that both concepts are related, the first being connected to the kinetics of the recombination reactions, the second being an empirical feature) is an open problem. In DSSCs, electrons can be transferred from the conduction band (free electrons) or from surface states located in the band gap of the oxide [131-132]. A recombination order lower than one is an empirical way of describing that electron transfer from the TiO_2 layer to I^{3-} ions may take place also from those occupied surface energy levels located in the energy gap [133]. However, a recombination through surface states is not only explanation for sub-linear recombination kinetics. A different rate of recombination can also arise from movements of the conduction band edge under illumination and kinetic complications due to the fact that reduction of tri-iodide is a two-electron process.

The most important indirect measurement of the conduction band electron density is the open circuit photovoltage (V_{oc}). The V_{oc} in any solar cell corresponds to the difference in electrochemical potentials (or Fermi energies)

of electrons in the contacts on each side [134]. The number of electrons in the conduction band can be derived from the density of states function $N_c(E)$ of electrons in the conduction band and the probability that an electron state is occupied $f(E)$ [135]

$$n_c = \int_{-\infty}^{+\infty} N_c(E)f(E)dE \quad 3-12$$

The probability of occupation is given by the Fermi-Dirac distribution function

$$f(E) = \frac{1}{1+\exp\left(\frac{E-E_F}{kT}\right)} \quad 3-13$$

where, E_F is the Fermi level, k the Boltzmann constant and T the absolute temperature. If we assume $E-E_F \gg kT$, we can apply the Boltzmann approximation to the Fermi Dirac distribution, which is reduced to [136]

$$f(E) \approx \exp\left(-\frac{E-E_F}{kT}\right) \quad 3-14$$

It is possible then to relate the Fermi level to the concentration of electrons in the conduction band by the expression [138]

$$n_c = N_c \exp\left(-\frac{E-E_F}{kT}\right) \quad 3-15$$

where N_c , as described above, is the effective density of states of electrons in the conduction band, E_c is the conduction band energy and E_F is the Fermi energy level in the oxide.

In the dark, electrons in the oxide (n_c^0) are in equilibrium with the electrolyte and the Fermi level in the oxide equals the redox potential, $E_{F,redox}$. The redox potential of the electrolyte solution is given by the Nernst equation:

$$E_{F,redox} = E^0 + \frac{RT}{nF} \ln \frac{[I_3^-]}{[I^-]} \quad 3-16$$

Where, R , T , n and F are the ideal gas constant, the temperature, the number of transferred electrons ($n = 2$ in this case (Equation 3-4)) and the Faraday's

constant respectively, and E^0 is the standard reduction potential of the I^-/I_3^- redox couple.

Under illumination (or externally applied bias), electrons in the oxide are no longer in equilibrium with the redox system and the electron density in the conduction band rises to a steady-state value. This steady-state electron concentration is determined by the balance between electron injection and electron transfer to I_3^- and the oxidized dye [137] and it defines the quasi-Fermi level (nE_F) of electrons [134] (Figure 3-5).

The open circuit photovoltage of the solar cell is then defined as the difference between the Fermi level in the dark and under illumination [138]

$$V_{oc} = n E_F - E_{F,redox} = \frac{kT}{q} \ln \left(\frac{n_c}{n_c^0} \right) \quad 3-17$$

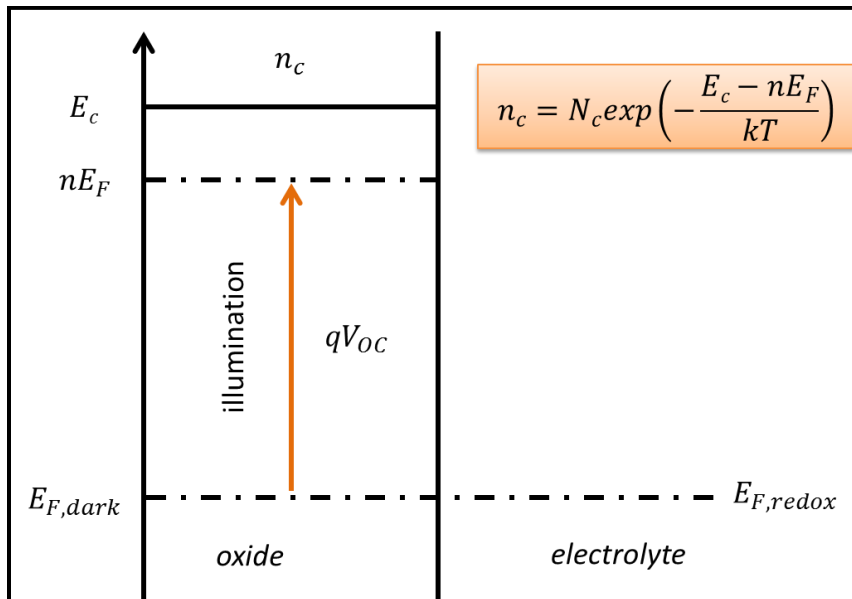


Figure 3-5 Energy level diagram of a DSSC under illumination at open circuit [124].

Thanks to the previous equation, the free electron concentration can be defined in terms of the open circuit voltage

$$n_c = n_c^0 \exp\left(\frac{qV_{oc}}{kT}\right) \quad 3-18$$

At open circuit conditions and under illumination, all injected electrons will recombine. Therefore

$$G = U_n \quad 3-19$$

Where, G is the generation rate, describing the rate of injection of electrons into the oxide (in units of electrons $\text{cm}^{-3} \text{s}^{-1}$). This generation rate is proportional to the intensity of the incident light (I_0). If we assume linear recombination kinetics, from Equations 3-6 ($U_n = k_r n_c$), 3-17 and 3-19 we get the following relation between photovoltage and light intensity:

$$V_{oc} \propto \frac{kT}{q} \ln I_0 \quad 3-20$$

This approximation predicts, therefore, that DSSCs should behave as an ideal diode [102], and a semilogarithmic plot of V_{oc} versus light intensity should give a linear response with a slope of 26 mV at room temperature. However, usually DSSC photovoltage varies with a slope higher than 26 mV and the empirical non-ideality factor m (Equation 3-2) accounts for this non ideality:

$$V_{oc} \propto \frac{mkT}{q} \ln I_0 \quad 3-21$$

Taking into account sub-linear recombination kinetics, the reaction order β would be related to the non ideality factor m by its inverse ($m = 1/\beta$), as can be obtained by combining Equations 3-11 ($U_n = k_r n c^\beta$), 3-19 and 3-21 above.

As commented before, the reasons for the non-ideality are not completely clear in the current literature. Apart from a reaction order different from one, it can arise from the fact that the relationship between the free electron concentration and the cell voltage as described in Equation 3-18 is only approximate. Some authors [137] have recently proposed an additional non-ideality parameter to describe the dependence of the conduction band electrons with Fermi level. This could be interpreted as a parameter modifying the effective concentration of free electrons in the conduction band (via an

electron activity) [139], or a parameter shifting the TiO₂ conduction band with electron concentration [140].

3.5.3 Photocurrent and incident photon to current efficiency

The short circuit photocurrent J_{sc} of a DSSC is determined by the overlap between its spectral incident photon to current efficiency (IPCE) and the spectral photon flux (I_0) of the incident illumination on the cell as shown in Figure 3-6 [141].

$$J_{sc} = q \int_{\lambda_{min}}^{\lambda_{max}} I_0(\lambda) IPCE(\lambda) d\lambda \quad 3-22$$

where λ_{min} and λ_{max} define a wavelength range. The IPCE can be calculated from the efficiencies of the processes that determine the electrical conversion in DSSCs by:

$$IPCE(\lambda) = \eta_{th}(\lambda) \eta_{inj}(\lambda) \eta_{col}(\lambda) \quad 3-23$$

Where, $\eta_{th}(\lambda)$ is the light-harvesting efficiency (or absorptance) of the sensitized oxide layer, $\eta_{inj}(\lambda)$ is the electron injection efficiency from the sensitizer into the oxide and $\eta_{col}(\lambda)$ is the electron collection efficiency.

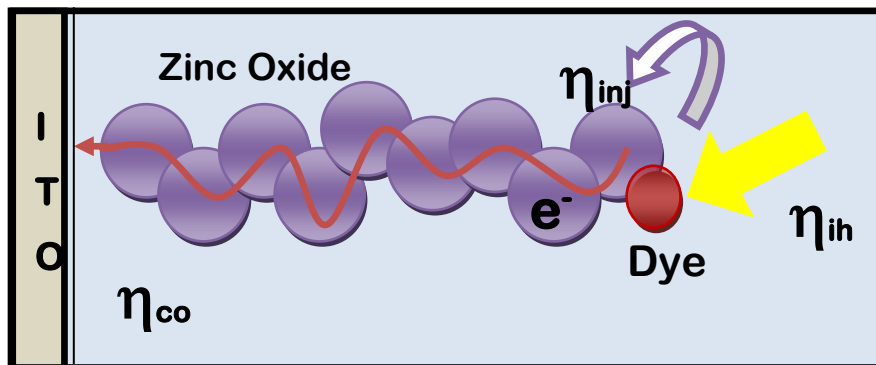


Figure 3-6 Scheme of processes, which determine the incident photon-to-current efficiency of DSSC [141].

The light harvesting efficiency or absorbance of the sensitized films indicates how efficiently the adsorbed dye molecules harvest the incident light. The electron injection efficiency (or injection quantum yield) corresponds to the

probability that a dye molecule in the excited electronic state injects an electron to the conduction band of the semiconductor. It thus determines how IPCE depends on charge separation at the dye/semiconductor interface. The charge separation depends on the driving force for electron injection from the LUMO of the dye to the conduction band of the semiconductor oxide, but also, as recently reported [142], on the populations of the acceptor and donor levels in the injection process and the corresponding back process (electron-dye recombination). Finally, the electron collection efficiency is an indication of the probability that a photogenerated electron reaches the collecting substrate contact before it is lost by recombination [141]. The collection efficiency thus depends on the average distance that electrons travel before recombination, which is expressed by a key parameter known as the electron diffusion length [143]. The photogenerated electron collection efficiency can be predicted by solving a continuity equation for electrons where generation, transport and recombination are taken into account simultaneously.

To mark the division of the IPCE into its optical and electrical parts, the absorbed photon to current conversion efficiency (APCE) can be defined. The APCE defines how efficiently absorbed photons are converted to electrons collected at the TCO substrate. The APCE is obtained by:

$$APCE(\lambda) = \frac{IPCE(\lambda)}{\eta_{th}(\lambda)} \quad 3-24$$

For state of the art DSSCs, the APCE reaches typically up to 100 % and the IPCE about 85% depending on reflection losses at the DSSC substrate [131].

3.6 Gas Sensors

3.6.1 ZnO based Gas Sensor

Semiconductor metal-oxide based gas sensors are commonly used for environmental monitoring and industrial applications due to their advantages such as small dimensions, low cost and convenient operation [144-145]. The

gas sensing mechanism of these sensors involves adsorption of atmospheric oxygen on the oxide surface that extracts electrons from the semiconducting material leading to change in carrier density and conductivity. On interaction with oxidizing or reducing gases, adsorbed oxygen concentration and thereby conductivity changes. The change in conductivity is a measure of gas concentration. Since the gas sensing mechanism is a surface reaction, use of nanostructured materials is expected to improve gas sensing characteristics.

Among the semiconductor metal oxides, zinc oxide (ZnO) is one of the most widely used gas sensing material [146-149]. ZnO is a very interesting material due to its high transmittance in the visible region and high chemical/thermal/mechanical stability [150]. The great advantage of using ZnO films in transparent electronic devices refer to the possibility of manufacturing high quality and transparent polycrystalline zinc oxide films at room temperature [151]. In this study, we present the work done in our laboratory on the growth of ZnO nano rod structures by sol-gel spin coating technique and detection of tea aroma and their gas sensing properties.

3.6.2 Detection of Tea Aroma

Tea is probably the most popular drink worldwide. Among all the beverages consumed worldwide, tea is a very popular one and used by all strata of people. There are several types of tea like black tea, green tea, Oolong tea etc., and out of these, black tea is the most common beverage. Black tea has two major varieties, viz., (1) Orthodox and (2) CTC (Cut–Tear–Curl operations are performed during production of this type of tea). For measurement of tea quality traditional methods of employing professional tea tasters are still being practiced, and unfortunately, no instrumental methods are deployed in the industry on regular basis. These tasters, based on their experience and judgment, assess the quality of tea and the pricing of tea are fixed accordingly. The tea-tasters give a mark in the range of 1 to 10 each for leaf quality, infusion and liquor of the sample [152]. This method is purely subjective and error-prone. Thus, there is a demand in the industry to have low-cost, portable

solutions for quality evaluation of black tea. In this regard, electronic nose has been demonstrated to be an appropriate candidate [153] for the same. The flavour in different commercial organic products like Tea, Coffee, Wine, etc. arises from Volatile organic compounds (VOC) emitted during infusion. VOCs are commonly used as ingredients in household products or in industrial processes where they normally get vaporized at room temperature and can be breathed, and unfortunately, many VOCs can cause adverse health effects [154]. Other synthetic products such as paints, wax or fuels can release toxic vapors when they are stored; even some foods, such as beverages, fish and meat products, emit organic vapours [155]. VOCs are also present in some workplaces, especially in the chemical industries; in these cases, it is important to monitor the concentration of the vapours to safeguard the health of the workers. They also keep atmospheric emissions under control in order to avoid environmental hazards. Finally, other inorganic gases such as hydrogen or oxygen also need to be monitored because of the high risk of explosions if their concentrations surpass safe levels. Due to all these reasons, sensing of VOC's has attracted increasing interest focused on their detection, monitoring and analysis. Porous nanostructured oxide materials like ZnO and SnO₂ have been studied extensively primarily for detection of inorganic gases [156]. Recently, ZnO have been extensively studied [157] for applications in practical gas sensing conversion devices [158]. ZnO is one of the potential semiconductor materials in sensor due to its fine physical, chemical and optical properties [158 - 160]. The most important aspect of the ZnO material is that it is completely an environment-friendly direct band gap material with wide bandgap energy of 3.37 eV and high exciton binding energy of ~60meV [161].

Another attractive feature of ZnO is that its bandgap energy can be engineered by changing dopant materials. ZnO, an n-type semiconductor, is also interesting due to its chemical and thermal stability. It can be grown at relatively low temperatures as compared to other wide band gap

semiconductors [161]. Inexpensive substrate and low temperature growth make these devices feasible to manufacture at a lower cost. However, these developments, in the mean time, demand a good reproducibility and clear understanding of the stability of thin film based multi-layered structures employed in the device design [162]. ZnO nanomaterial also appears to be the mostly studied one as it exhibits a wide variety of nanostructures such as nanowires [155], nanowalls [156-157], nanobelts [157], nanorods [159], nanosheets [159], and so on.

Recent research has demonstrated that the ZnO nanostructures is highly oriented and ordered arrays is of crucial importance for the development of novel devices [160]. It has been recognized as one of the promising nanomaterials in a broad range of high technology applications, e.g., surface acoustic wave device [155], chemical sensor [156], photonic crystals [163], light emitting diodes [164], varistors [157], and photoanode films of solar cell [158-159]. Among its applications, ZnO nanowire is receiving greater interests for fabricating sensors for detection of VOCs, for example, ethanol. ZnO nanowires prepared by a reactive thermal deposition method were used for ethanol sensing [160]. Very recently, nanocrystalline ZnO gas sensors have attracted more interest due to their better properties of detecting pollutants, toxic gases, alcohols and food freshness, especially fish freshness [165], or as gas-sensing films integrated on one chip to make an “electronic nose” [166]. The sensitivities of gas sensors can be greatly improved by doping Fe^{+3} , Co^{+3} and Ni^{+2} . In some recent paper, identification of flavour components through pattern recognition analysis [167-168], of Chinese liquors was carried out using doped nano ZnO gas sensor array and different statistical techniques were compared for their classification ability [170].

3.6.3 Electronic Nose systems

The E-nose system is a fast and cost effective solution to the problems associated with both of the conventional methods of tea quality determination based on organoleptic study and chemical analysis. The system consists of an

array of gas sensors which record the characteristic response for a particular odour and the pattern recognition methodologies, in form of software to identify the odour using the sensor response data set [170].

The E-nose systems are usually designed to mimic the functioning of mammalian olfactory systems. A typical E-nose device consists of an array of sensors, signal conditioning unit and pattern recognition unit. Using different sampling techniques like head space sampling, diffusion methods, bubblers or pre-connectors the odour molecules are carried on to the sensor array. The sensing materials upon contact with the odour molecules suffer some physico-chemical changes, leading into the change in their electrical properties such as conductivity. Each sensor in the array responds to different odour molecule in a varying degree and results into difference in the responses. The total set of responses from all of the sensors are then transduced into electrical signals and used for pattern recognition after pre-processing and preconditioning [171-172].

In modern E-nose systems a variety of sensors like Conductivity sensors, Conducting polymer composite sensors, Intrinsically conducting polymers, Metal oxide sensors, Piezoelectric sensors, Surface acoustic wave sensor, Quartz crystal microbalance sensor, Optical sensors, Metal-oxide-semiconductor field-effect transistor sensor etc. are usually used in the array depending upon the chemical composition of the odour/odour mixtures. Gas molecules interact with solid-state sensors by absorption and with thin or thick films of the sensor materials by adsorption or chemical reactions. These changes in the sensing materials are measured as electrical signals and considered as responses. The most common types of changes utilised in e-nose sensor systems are shown in Table-3-3 along with the classes of sensor devices used to detect these changes.

Table 3-3 Physical changes in the sensor active films and the sensor devices used to transduce them into electrical signals [170].

Physical changes	Sensor devices
Conductivity	Conductivity sensors
Mass	Piezoelectric sensors
Optical	Optical sensors
Work function	MOSFET sensors

In the first stage of odour analysis by E-nose system a reference gas, usually inert gases like nitrogen was flushed through the array of sensors, and then the odour is allowed to reach the sensors. After data recording is completed the reference gas is again flushed through the sensors. The reference gas was flushed before and after the analysis to prepare the base line of responses. The period of time when sensors are exposed to odour is called response time, and the time when reference gas is passed through it, is called the recovery time. Once the responses are recorded, it is then processed for pattern recognition after the base line correction [171].

The basic data analysis techniques employed for pattern recognition in E-Nose system fall into three major types:

1. **Graphical analysis:** bar chart, profile, polar and offset polar plots.
2. **Multivariate data analysis (MDA):** principal component analysis (PCA), canonical discriminate analysis (CDA), featured within (FW) and cluster analysis (CA).
3. **Network analysis:** Artificial Neural Network (ANN) and Radial Basis Function (RBF).

The choice of method depends on type of responses obtained and purpose of its use [173].

3.6.4 Quality determination of Orthodox Tea by E-nose systems:

A Neural Network based E-nose, comprising of an array of four tin-oxide gas sensors, can assist tea quality monitoring during quality grading. Principal Component Analysis (PCA) was used to visualise the different aroma profiles

was proposed in 2008 [178]. In addition, K-means and Kohonen's Self Organising Map (SOM) cluster analysis was done. Subsequently other analytical methods like, Multi Layer Perceptron (MLP) network, Radial Basis Function (RBF) network, and Constructive Probabilistic Neural Network (CPNN) were used for aroma classification [170 - 171].

A metal oxide sensor (MOS) based electronic nose (EN) to analyze five tea samples with different qualities, namely, drier month, over fired drier month, well fermented normal fired in oven, well fermented over fired in oven, and under-fermented normal fired in oven using an array of 4 MOSs, each of which has an electrical resistance that has partial sensitivity to the headspace of tea, and a suitable interface circuitry for signal conditioning was proposed by Dutta *et al.* [153]. The data were processed using Principal Components Analysis (PCA), Fuzzy C means algorithm (FCM). The use of a Self-Organizing Map (SOM) method along with a Radial Basis Function network (RBF) and a Probabilistic Neural Network classifier was also explored. Using FCM and SOM feature extraction techniques along with RBF neural network 100% correct classification was achieved for the five different tea samples with different qualities viz. over-fermented, overfired, under-fermented, etc. [174].

A support vector machine algorithm to be superior to KNN, and ANN model for green tea quality gradation by E-nose with MOS sensors, and it could be successfully used in discrimination of green tea's quality was proposed by Chen *et al.* [175]. The study was undertaken for classification of four different grades of green tea classified by human sensor panel. Principal component analysis (PCA) and three different linear or nonlinear classification tools viz., K-nearest neighbors (KNN), artificial neural network (ANN) and support vector machine (SVM), were compared in developing the discrimination model [175] extracted the principal components (PCs), as the input of the discrimination model.

The electronic nose (E-nose) was employed for identification of quality grades of green tea, applying BPNN, PNN and cluster analysis (CA) by Yu *et al.* [176]. Principal components obtained by principal component analysis (PCA) were extracted as the inputs to the BPNN and PNN. Results of CA showed that the classification of the different green tea samples is possible using the response signals of the E-nose. BP neural network was reported to give better experimental results. For the two neural networks BPNN and PNN, the classification success rates were reported 100% and 98.7% for the training set, and 88% and 85.3% for the testing sets respectively. As the overall results of the experiment, it was reported that the two neural networks are usable for identification of the different green tea samples [177].

The incremental-learning fuzzy model to classify black tea using E-nose instrument, since incremental learning is not possible in commonly used classification algorithms was proposed by Tudu *et al.* [177]. The proposed incremental learning fuzzy model promises to be a versatile pattern classification algorithm for black tea grade discrimination using electronic nose. The algorithm has been tested in some tea gardens of northeast India, and encouraging results have been obtained [178].

In our study, doped and un-doped ZnO nanorods based sensor have been developed and characterized. The fabricated sensor element was tested for its resistive response for evaluation of quality of two different types of tea infusion Orthodox and CTC. The performance of the sensor elements was characterized in different temperature of operation of the sensor element and different sensor characteristics were evaluated. Keeping in view of the small variation of the resistivity with changing gas environment, the response was detected through an appropriate circuit in order to improve its sensitivity. A Wheatstone bridge circuit was used with compensation of cross sensitivity due to temperature variation of the sensor element as shown in Figure 4-4.

CHAPTER 4

4. MATERIALS AND METHOD

4.1 Steps for fabrication of ZnO based devices

Main steps followed to study zinc oxide based materials, both as nanorods and thin films are:

- Synthesis of ZnO nano-rods using sol-gel spin coating methods;
- Deposition of ZnO, doped ZnO and on ITO thin films substrates (2cm × 2cm);
- Coating electrodes by screen printing technique for DSSCs and Sensors
- The Fabrication of ZnO based Dye sensitized solar cells.
- Fabrication of doped ZnO nanorod sensors for electronic nose

4.1.1 Fabrication of ZnO Nanorods

Synthesis of ZnO nanorod Spin-coating is a simple method for preparing ZnO nanoseed from Zinc acetate solution. In this process, we prepared 5mM solution of Zinc acetate dehydrate, $(\text{CH}_3\text{COO})_2\text{Zn}$, $2\text{H}_2\text{O}$, (98% Merck) with methanol. The mixture was well mixed using an ultrasonic bath for 1 hour and then the resultant paste was dropped over a glass plate and the solution spun at 1000 rpm for 30s using a Programmable Spin Coater (Apex Technologies, Model SCU-2008C). Thus the nano layer of Zinc acetate solution is spread uniformly on a rotating substrate [179]. The coated substrates were heated to 350°C in conventional oven for 30 min to yield layers of ZnO islands with their (100) plane parallel to the substrate surface [179]. After evaporation of solvent, a thin ZnO film was formed whose thickness can be controlled by repeating the above process. Concentration of the solution in the spin coater and spinning rate of the substrate also play important roles in adjusting the thickness of the formed seed layer. For preparing ZnO nanorods standard sol-

gel protocol was used [180]. ZnO nanoseed were immersed in a solution with Zinc acetate and Hexamine in same proportion and kept at 90°C for 2 hours for growth of nanorods. This forms an array of vertically aligned ZnO nanorods on the substrate surface. The coated substrate is rinsed and electrode with silver paste for further analysis.

ZnO thin films were prepared by the sol-gel spin coating method. As a starting material, zinc acetate dehydrate ($\text{Zn}(\text{CH}_3\text{COO})_2 \cdot \text{H}_2\text{O}$) was used. 2-methoxyethanol and MEA were used as a solvent and stabilizer, respectively. The dopant sources of Fe, Co and Ni were Fe- Acetate, Co-Acetate and Ni-Acetate respectively. Zinc acetate dihydrate and a dopant were first dissolved in a mixture of 2-methoxyethanol and MEA solution at room temperature. The molar ratio of MEA to zinc acetate was maintained at 1.0 and the concentration of zinc acetate was 0.35 M. The solution was stirred at 60 °C for 2 h to yield a clear and homogeneous solution, which served as the coating solution after cooling to room temperature. The coating was usually made 2 days after the solution was prepared.

The solution was dropped onto glass substrates, which were rotated at 3000 rpm for 30 s. After depositing by spin coating, the films were dried at 350 °C for 30 min over a conventional furnace to evaporate the solvent and remove organic residuals. The procedures from coating to drying were repeated six times until the thickness of the sintered films was approximately 200 nm.

The crystallinity of each ZnO film was measured using an X-ray diffractometer with $\text{CuK}\alpha$ radiation. The surface and cross-section of the films were observed with a scanning electron microscope (SEM). The electrical resistance was measured by a four-point probe method. Optical transmittance measurements were carried out using a UV–VIS spectrophotometer.

4.1.2 Doping of ZnO

Sol-gel spin-coating is a simple method for preparing ZnO nanoseed from Zinc acetate solution to finally synthesize ZnO nanorods. In this process, we prepared 5mM solution of Zinc acetate dehydrate, $(\text{CH}_3\text{COO})_2\text{Zn} \cdot 2\text{H}_2\text{O}$, (98% Merck) with methanol. The mixture was well mixed using an ultrasonic bath for 1 hr and then the resultant paste was dropped over a glass plate and the solution spun at 1000 rpm for 30s using a Programmable Spin Coater (Apex Technologies, Model SCU-2008C). Thus the nano layer of Zinc acetate solution is spread uniformly on a rotating substrate. The coated substrates were heated to 350°C in conventional oven for 30 min to yield layers of ZnO islands with their (100) plane parallel to the substrate surface [180]. After evaporation of solvent, a thin ZnO film was formed whose thickness can be controlled by repeating the above process. Concentration of the solution in the spin coater and spinning rate of the substrate also play important roles in adjusting the thickness of the formed seed layer. To prepare ZnO nanorods, standard sol-gel protocol was used [180]. ZnO nanoseed were immersed in a solution with Zinc acetate and Hexamine in same proportion and kept at 90°C for 2 hours for growth of nanorods. This forms an array of vertically aligned ZnO nanorods on the substrate surface. The coated substrate is rinsed and electrode with silver paste for further analysis.

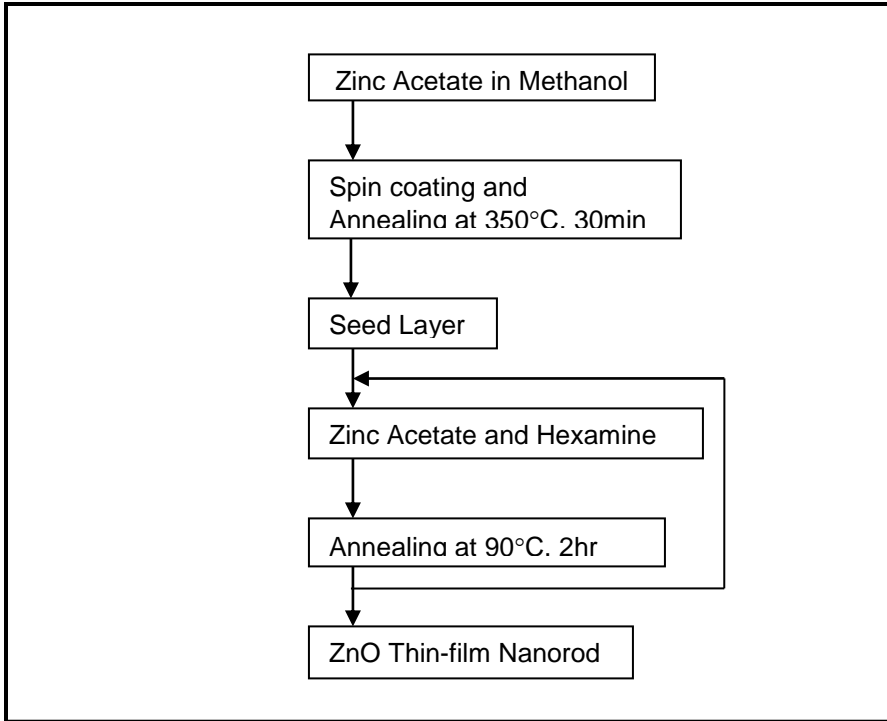


Figure 4-1 Flow chart for preparation of ZnO nano layer.

A flow diagram of total synthesis process of ZnO nanolayer as presented in Figure 4-1. The formation of phases were ascertained through study of x-ray diffraction pattern of the film calcined at various temperatures. Results showed pure ZnO phase formed at 350°C and above. For proper microstructure of sensor element, 350°C was taken as optimum sintering temperature. The fabricate sensor material is characterized through SEM and the picture Figure 5-3 shows clear ZnO nanorods aligned vertically perpendicular to substrate plane. Fabrication of device structure and measurement two interpenetrating comb like electrode structures were made with silver paste on the deposited film and was cured at 150°C. Finally, two

electrodes were soldered with copper wires for connecting with Whetstone Bridge circuit for measurement of off-balance voltage due to resistance change of the element.

For preparation of doped ZnO, Fe-Acetate, Co-Acetate and Ni-Acetate were added with Zinc acetate with appropriate proportion with further steps being identical to fabrication of the undoped one. The resulting nano-layer produced in this method over the substrate was electrode and connected to a digital multimeter for measuring the simultaneous resistance change in an atmosphere whose flavour (VOC composition) has to be determined.

4.2 Fabrication of Dye Sensitized Solar Cells

4.2.1 Steps for fabrication

At first, ZnO nanorod was synthesized using sol-gel method and fabricated using Spin coating technique. Spin-coating is a simple method for preparing ZnO nanoseed from Zinc acetate solution. In this process, we prepared 5 mM solution of Zinc acetate dehydrate, $(\text{CH}_3\text{COO})_2\text{Zn} \cdot 2\text{H}_2\text{O}$, (98% Merck) with methanol. The solution was spun on indium tin oxide (ITO)-coated glass substrates at 1000 rpm for 30s. The Zinc acetate solution is spread on a rotating substrate [181-182]. The substrates were heated to 350°C in conventional oven for 30 min to yield layers of ZnO islands with their (100) plane parallel to the substrate surface. After evaporation of solvent, a thin ZnO film was formed. Repetitions of the above process 5 to 7 times were carried out to control the thickness of the film. Concentration of the solution and spinning speed of the substrate also play important roles in adjusting the thickness of the fabricated film. The counter electrode (cathode) was prepared on another ITO coated glass by using carbon dust.

4.2.2 Dye Deposition

The device was immersed in a solution of sensitized dye for 24 hours to allow the dye molecules to covalently bond to the surface of the ZnO. The sample

were then rinsed with ethanol to remove excess dye on the surface and air-dried at room temperature. The absorption spectra of dyes were recorded using a UV–Vis spectrophotometer (Perkin Elmer Lamda-35).

4.2.3 DSSC assembling

DSSCs were assembled following the procedure described in the literature [181]. The carbon dust coated counter electrode was placed on the top so that the conductive side of the counter electrode faces the ZnO film. The iodide based solution as the liquid electrolyte (0.5M potassium iodide mixed with 0.05M iodine in water-free ethylene glycol) was placed at the edges of the plates. The liquid was drawn into the space between the electrodes by capillary action. Two binder clips were used to hold the electrodes together.

4.2.4 Apparatus Setup

Keithley model 2400 digital source multimeter was used to measure the dark-light and illuminated *I-V* curves of the DSSC under white light illumination (Xenon-lamp) condition were recorded during the efficiency measurement experiments. The position of the light source was adjusted such that the light intensity is 100 mW/cm^2 (the equivalent of one sun) at AM 1.5 of power was delivered to the surface of the measured DSSC solar cell. The current voltage characteristics of DSSCs under various light intensities were obtained. Photograph of fabricated setup for measuring Sensor responses is presented in the picture below.

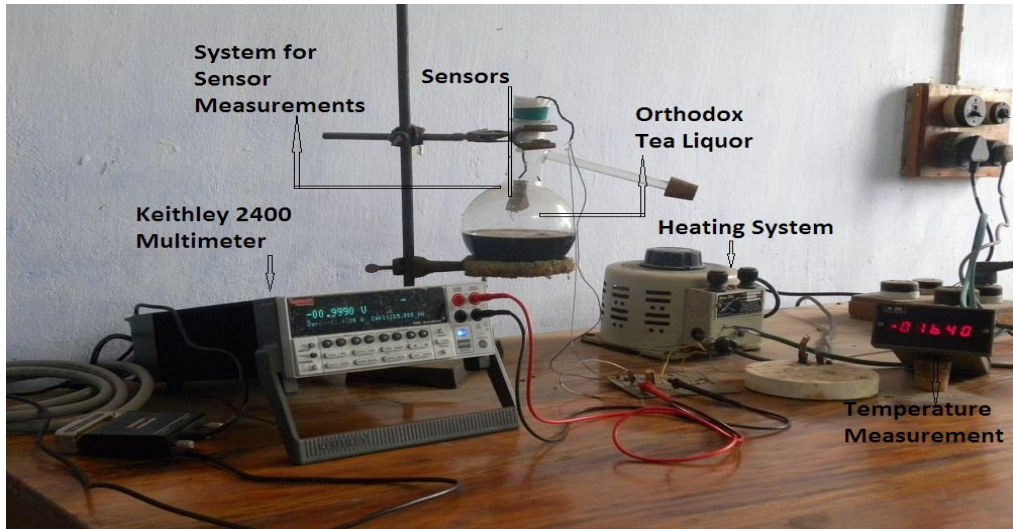


Figure 4-2 Keithley 2400 Multimeter connected with computer system for sensor measurements.

4.3 Gas Sensors Measurements

Dry tea leaves were weighed (10g) and placed in a glass flask and appropriate amount (500 ml) of water were added as shown in Figure 4-3. Finally, the sample was heated at 100°C while measurement of output voltage of the circuit was carried out.

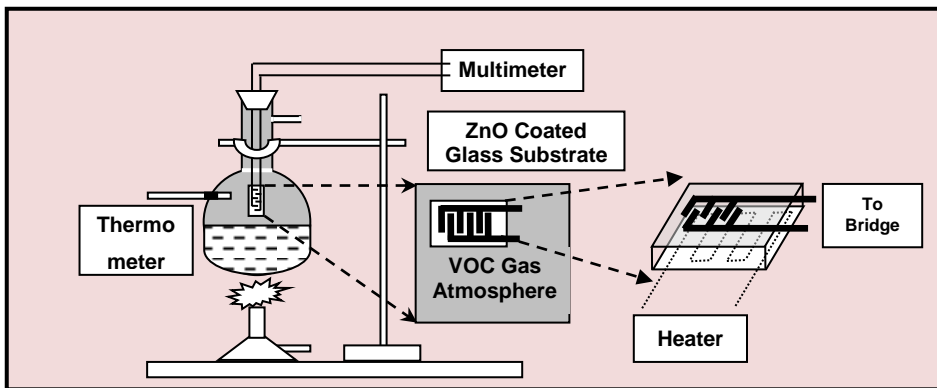


Figure 4-3 Sample measurement system in static gas environment.

The output for the sensor is connected to a Whetstone bridge circuit consisting of a resistance (of same order of resistance of sensors) a variable resistance (for bridge balancing) and two sensors, one for measurement and one for temperature compensation as shown in Figure 4-4.

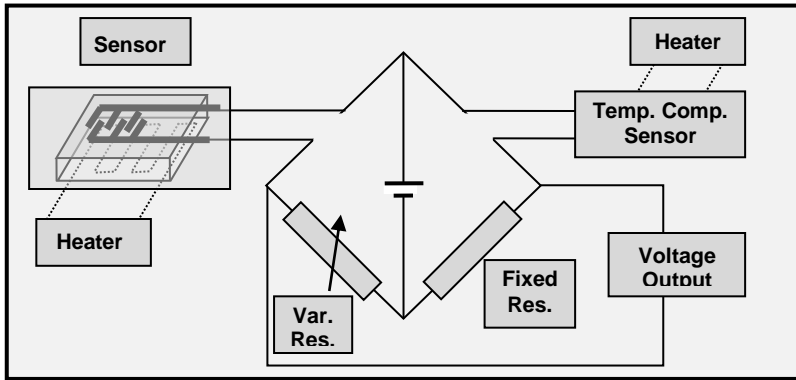


Figure 4-4 Schematic diagram of circuit and device connection for sensor measurement.

The resistances are of same order of the sensor elements while the variable resistance was adjusted for balancing of the bridge. Two exactly similar sensor elements heated simultaneously at same temperature were connected at other two arms of the bridge. One of the element being placed in the gas environment (tea infusion), while the other in open atmosphere. The bridge was powered through a dc power supply (12V).

4.4 Sensor Array and its Responses in Tea Infusion Vapour

For fabrication of E-nose, four such sensor measurement units, one of pure ZnO, one doped with iron, one doped with cobalt and one doped with nickel were incorporated at the same time in tea infusion vapour and the change of resistances of individual sensor were detected simultaneously.

Four major grades of Orthodox black tea samples, Leaf, Broken, Fannings and Dust, were collected from 14 Darjeeling tea gardens.

4.5 E-Nose measurements

This includes investigation on various sensors and sensor arrays useful for detection of smell and visual appearance of black tea liquor by electronic means using the system. Individual sensor circuitry is shown as sketch diagram in Figure 4-4. Four similar system in inserted in infusion vapour for simultaneous measurement. These E-Nose sensor responses of Volatile Organic Components (VOC) emitted from heated tea samples were analyzed through a Principle Component Analysis as presented in details in the results section.

4.6 Correlating sensor signals with Tea-tasters scores

The made tea samples were sent to selected professional tea tasters for organoleptic evaluation, and scores (between 1 to 10) were obtained for strength, aroma, and colour of the liquors. The evaluation included estimation of following parameters: Colour with milk, Colour without milk, Colour of Infused Leaf, Strength, Flavour and Price/Kg.

The Flowchart of experimental processes to calibrate the sensing parameters and tea taster's scores are outlined in the Figure 4-5.

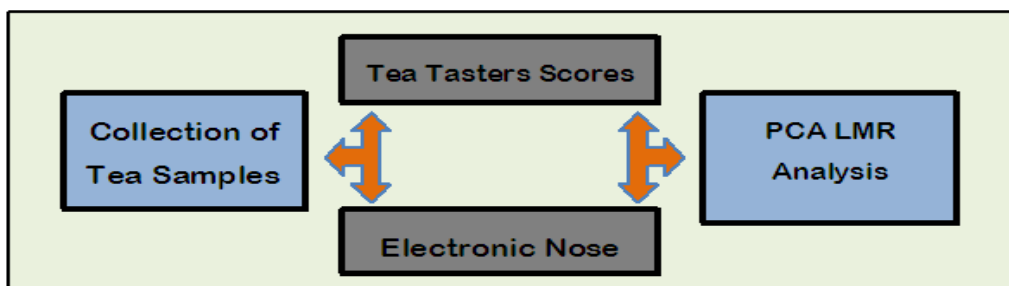


Figure 4-5 Sketch of the Electronic Nose system used for the study.

CHAPTER 5

5. RESULTS AND DISCUSSION

5.1 ZnO and its characteristics

5.1.1 X-ray Diffraction Analysis

The ZnO thinfilm crystal structure was investigated by X-ray diffraction analysis (Philips X'Pert Pro Alpha1 MPD diffractometer), utilizing Cu-K α_1 radiation ($\lambda=0.15406$ nm). Figure 5-1 shows the X-ray diffraction patterns of ZnO thin film. The EDAX analysis of selected area of SEM image was also studied for analysis of purity and identification of phases. Analysis shows a little impurity containing La ions. X-ray diffractogram of ZnO films doped with iron, cobalt and nickel were also studied. However, no significant departure in the diffractogram from that of pure ZnO was noticed.

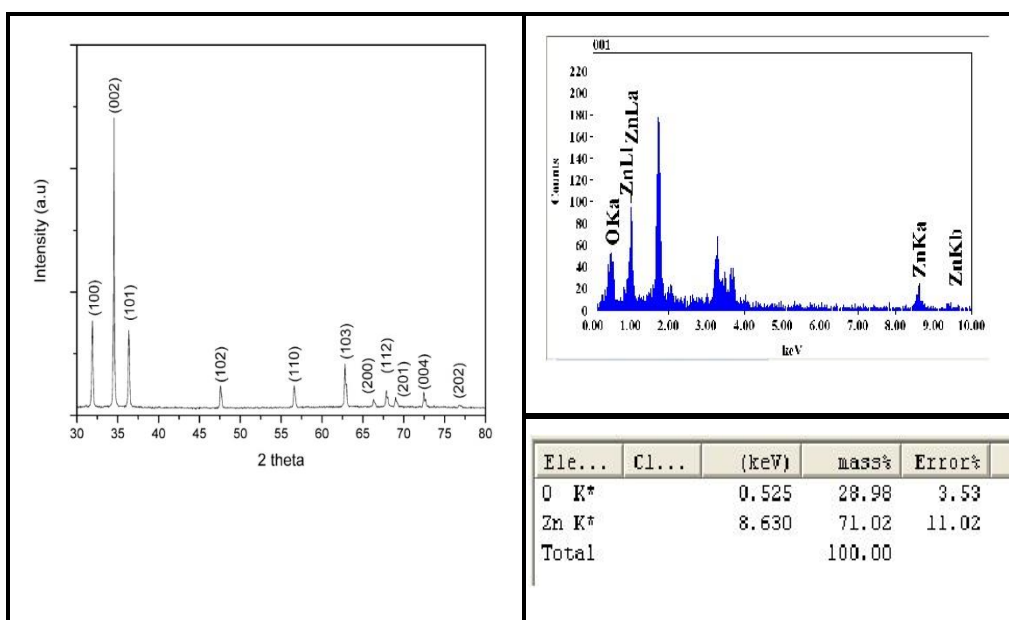


Figure 5-1(a) X-ray diffraction patterns of ZnO thin film and (b) EDX analysis of ZnO Sample

5.1.2 Effect of Dopant Concentration

The surface morphology of the films and its dependency on the type and concentration of the dopant are displayed in Figure 5-2.

A particular structure was observed in SEM images of doped and un-doped ZnO thin films on glass substrates for all films. The particle size of films doped with 1 at.% for all dopants was somewhat larger than that of the un-doped film. In the case of Co doping, the film doped with 1 at.% exhibited a porous structure and had grain sizes of 150 nm on the average. The microstructure of the films consisted of many round shaped particles. In addition, the films had a smooth surface morphology.

For the Fe doped films, the film have even larger grains. The grain size of the 1 at.% Fe doped film reduced a little, but the packing density of the film increased due to disappearing gaps between particles. The grains are more flaky in nature reducing the overall surface area.

For Co-doped films, particles with different shapes and sizes were mixed. Additionally, a microstructure with a larger difference in size between the large and small particles, similar to the case of Ni-doped film was observed. In the cases of films doped with Co and Ni with a smaller ionic radius than zinc, particles forming a matrix became smaller with increased doping concentration because grain growth was disturbed by compression stresses due to the difference in ionic radii between zinc and Co or Ni. The change in particle size with an increase in doping concentration was observed more in the Co-doped films than in the Ni doped films. This is due to a higher difference in ionic radius between zinc and Co than that of the radii of zinc and Ni. However, since the ionic radius of Fe was larger than that of zinc, the change in particle size with an increased dopant concentration for Fe was less than that for the other dopants.

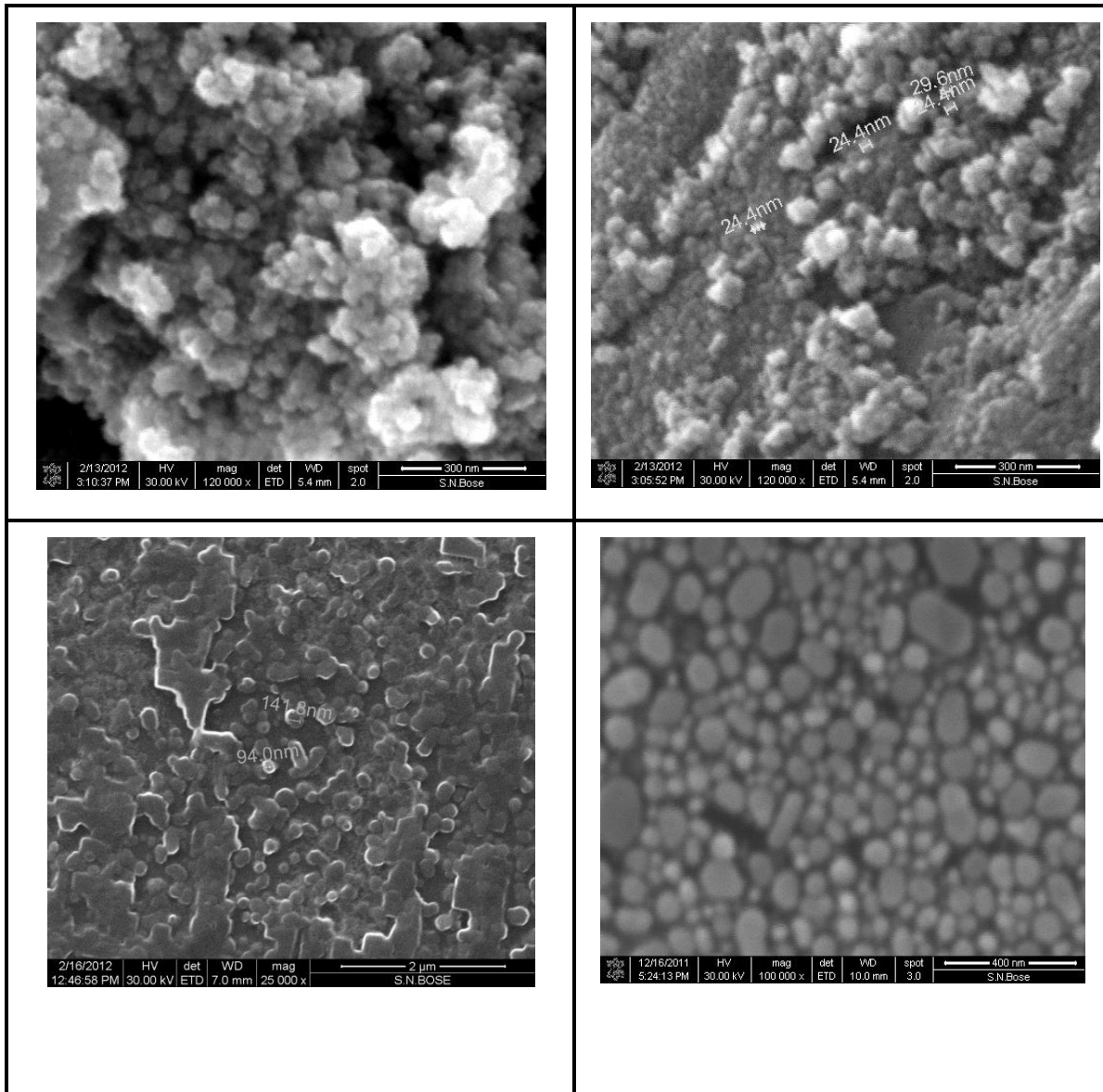


Figure 5-2 SEM images of un-doped and doped ZnO thin films with (a) Undoped ZnO (b) Fe doped ZnO (c) Co doped ZnO and (d) Ni doped ZnO

The electrical resistivity of doped films was decreased by an increase in the carrier concentration. The lowest electrical resistivity values of the doped films were found out to be 1.1×10^{-1} , 4.8×10^{-1} and $5.6 \times 10^{-1} \Omega\text{cm}$ for Fe, Co and Ni, respectively. However, the increase in the electrical resistivity of doped films with increasing doping concentration may be due to a decrease in mobility of carriers caused by segregation of dopants at the grain boundary. Doped materials were acting as an electrical dopant at initial doping concentration but as an impurity at more doping concentrations having the lowest electrical resistivity values. Additionally, the electrical resistivity value of film was inversely proportional to a (0 0 2) preferred orientation of film. The resistance was measured using a Keithley 2400 multimeter configured in the two-wire mode. The main electrical characteristics: conductivity, carrier concentration, and mobility were derived from Hall measurements [184].

Table 5-1 Properties of doped and undoped sensing elements

	ZnO Film	Fe doped ZnO	Co doped ZnO	Ni doped ZnO
Average Grain Size (nm)	120	120	200	150
Surface Resistivity ($\Omega\text{-cm}$)	2.4×10^{-1}	1.1×10^{-1}	4.8×10^{-1}	5.6×10^{-1}
Electron mobility ($\text{cm}^2/\text{V s}$)	17.1	14.3	12.1	11.2
Conductivity ($\Omega \text{ cm}$) ⁻¹	0.015	21.981	1.651	0.001
Electron concentration (cm^{-3})	5.8×10^{15}	9.1×10^{18}	8.6×10^{17}	9.73×10^{14}
Semiconductor Band Gap (from UV-Vis abs. spectra) (eV)	3.31	3.27	3.29	3.27

The UV-Vis absorption spectra, carried out between wavelengths from 300 to 800 nm, of the un-doped and doped ZnO thin films. The band gap were measured through the general formula given by Davis and Mott [185] for optical band gap E_g is

$$\alpha h\nu = [B(h\nu - E_g)]^r \quad 5-1$$

where, r = index taking different values depending on the mechanism of the inter band transition (usually 2 for ceramic system), B = constant called band tailing parameter and $h\nu$ = incident photon energy.

Therefore for undoped and doped ZnO equation (5-1) becomes

$$\alpha h\nu = [B(h\nu - E_g)]^2$$

or, $(\alpha h\nu)^{1/2} = Bh\nu - BE_g$

Variation of $(\alpha h\nu)^{1/2}$ with $h\nu$ will be straight line having slope $m = B$ and intercept $c = BE_g$

Therefore $E_g = BE_g / B = c/m = \text{intercept/ slope}$

The results of Hall measurements band gap studies were presented in Table 5.1.

5.2 Dye Sensitized Solar Cell

5.2.1 Structure Characterization

The morphology of the samples was observed using a scanning electron microscope (SEM) with a field emission gun operating at 200 kV. Figure 5-3 displays ZnO nanowire arrays in a wide surface area. The nanorods have an average length of 600 nm, diameter ranging from 100 to 200nm and they are mostly vertically aligned with the substrate having hexagonal shapes. The thickness of ZnO film was around $\sim 2 \mu\text{m}$.

The nanowires, which make barrier free contact with the substrates, exhibit resistivity around 0.3 to 2.0 Ωcm along the long axis [186]. The nanowire used in the present work had a resistivity 0.7 Ωcm at 0V. Due to absence of interfaces in nanowires, resistivity of a nanowire should be lower than nanoparticle thin films. Moreover, conductivity in the nanowire arrays increases by 5 to 20% when they are soaked in standard DSSC electrolytes [187].

In general, the energy conversion efficiency of ZnO based DSSCs is lower than that of TiO₂ DSSCs [186]. However due to the barrier free contact, ZnO nanowire is expected to give higher efficiency. Because only about 4% of the solar spectrum falls in the UV region, ZnO semiconductor absorbs solar radiation while sensitized by natural dye molecules with absorption spectra at visible region.

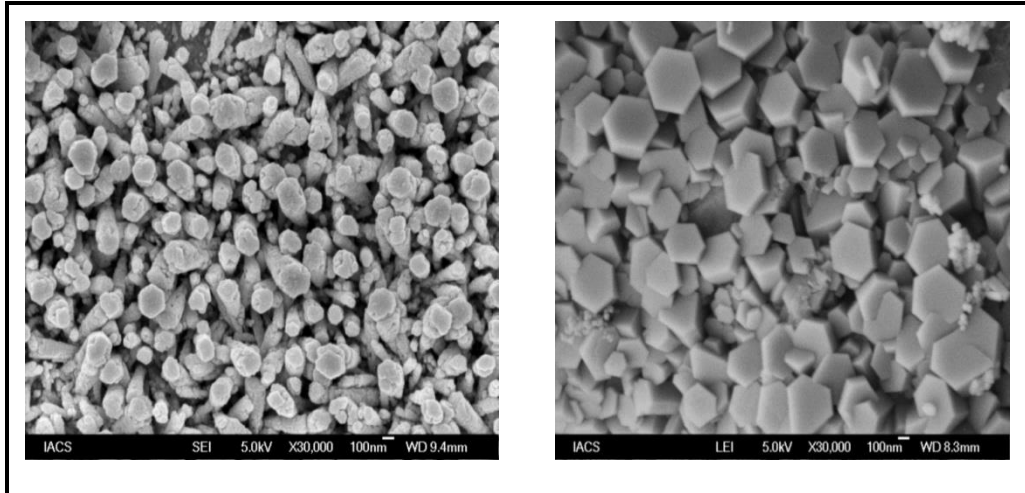


Figure 5-3 Scanning electron microscope (SEM) picture of ZnO nanorod used in DSSC

Anthocyanin dyes present in Pomegranate Fruits are responsible for absorption of solar energy [188]. Anthocyanin dye is responsible for several colors in the red–blue range depending on pH value. The red anthocyanin absorbs at 530 nm (band gap 2.3 eV). Whereas, Rose Bengal has got a Xanthene class of dye with a band gap 1.9 eV and maximum absorption peak at 555 nm.

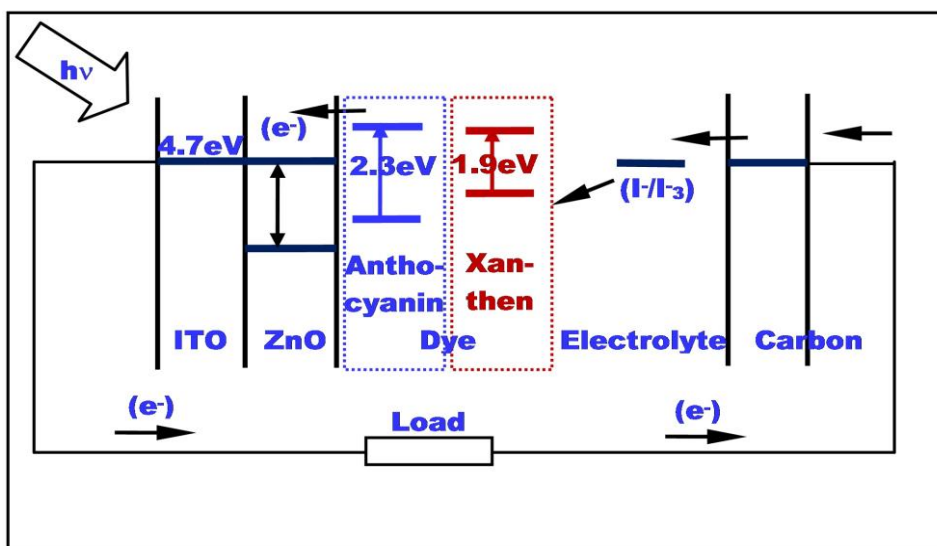


Figure 5-4 Working Principle of DSSC with Various Dyes

After absorbing photon energy from the illuminated white light, the dye molecules in the DSSCs become excited and inject electrons to the ZnO nanowires (Figure 5-4). Due to favorable energy difference, electron transfer occurs between the lowest unoccupied molecular orbital (LUMO) of the dye and the conduction band of ZnO. The photo-generated electrons percolate rapidly through the ZnO nanowire and are collected by the conducting glass support. The highest occupied molecular orbital (HOMO) of the dye is energetically lower than the redox potential, E_{redox} of the iodine/triiodide couple. The energy difference provides the driving force for hole injection into the electrolyte as presented in Figure 3-5. Recombination of charge carrier is also minimized in such devices since transport of only one type of carrier (electron, in general) is energetically possible from the dye to the semiconductor. For Rose Bengal dye (Xanthenes), the energy difference is 1.9 eV and for pomegranate (Anthocyanins) the energy difference is 2.3 eV [181].

5.2.2 Characteristics of Dye-Sensitized solar cells

Current–voltage characteristics of a cell in dark and under illumination permit an evaluation of most of its photovoltaic performances as well as its electric behavior [189]. The short circuit current I_{sc} is the one which crosses the cell at

zero applied voltage and it is a function of illumination. Charges travel under an internal potential difference typically equal to V_{oc} .

The open circuit voltage is measured when current in the cell is 0, corresponding to almost flat valence and conduction bands; I_{max} and V_{max} values are defined in order to maximize the power $|I_{max} \times V_{max}|$. This is the maximum power P_{max} delivered by the cell.

Fill factor FF is the ratio of the maximum power to external short and open circuit values:

$$FF = \frac{P_{max}}{V_{oc} \times I_{sc}} = \frac{I_{max} \times V_{max}}{I_{sc} \times V_{oc}} \quad 5-2$$

The external photovoltaic yield or efficiency η is defined as the ratio of the maximum electric power extracted to the illumination times the surface area, i.e. P_{in} of the cell:

$$\eta = \frac{V_{oc} \times I_{sc} \times FF}{P_{in}} \quad 5-3$$

(it is often expressed as a percentage). Conversion yield is the key parameter as concerns cells productivity [189].

5.2.3 The Equivalent Circuit Model of DSSC

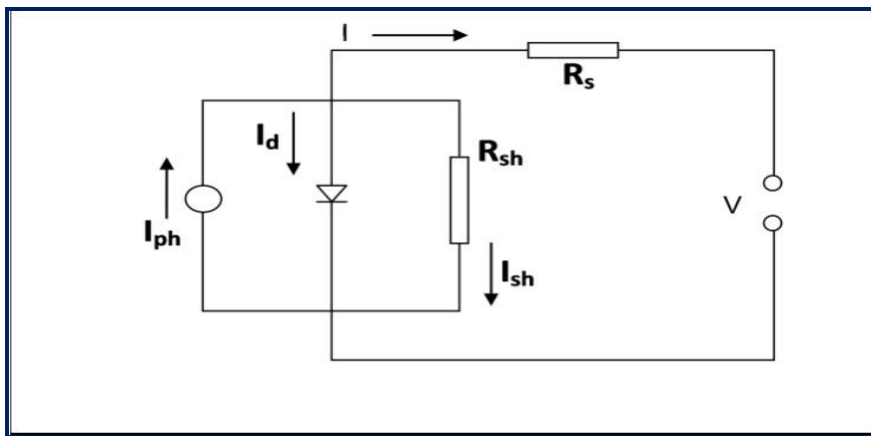


Figure 5-5 Equivalent Circuit Diagram of DSSC.

A solar cell is generally characterized using the equivalent circuit of the single diode model as shown in Figure 5-5 and the relation between the current I and the voltage V is given by

$$I = I_{ph} - I_s \left[\exp \left\{ \frac{q(V + R_s I)}{A k_B T} \right\} - 1 \right] - \frac{V + R_s I}{R_{sh}} \quad 5-4$$

where I_{ph} , I_s , R_s , R_{sh} , q , A , k_B , and T are the photocurrent, the saturation current of the diode, the series resistance, the shunt resistance, the electron charge, the ideality factor, the Boltzmann constant, and absolute temperature, respectively.

5.2.4 Characterization of Dyes

Three organic dyes, which are commonly used to sensitize the semiconductor layer in DSSC, are Rose Bengal, Pomegranate and Mixed Dye having absorption peak at 555, 525, and 545 nm, respectively as shown in Figure 5-6. These dyes suffer from the fact that individually they absorb very small portion of the visible spectrum of solar radiations giving rise to a low efficiency of DSSCs.

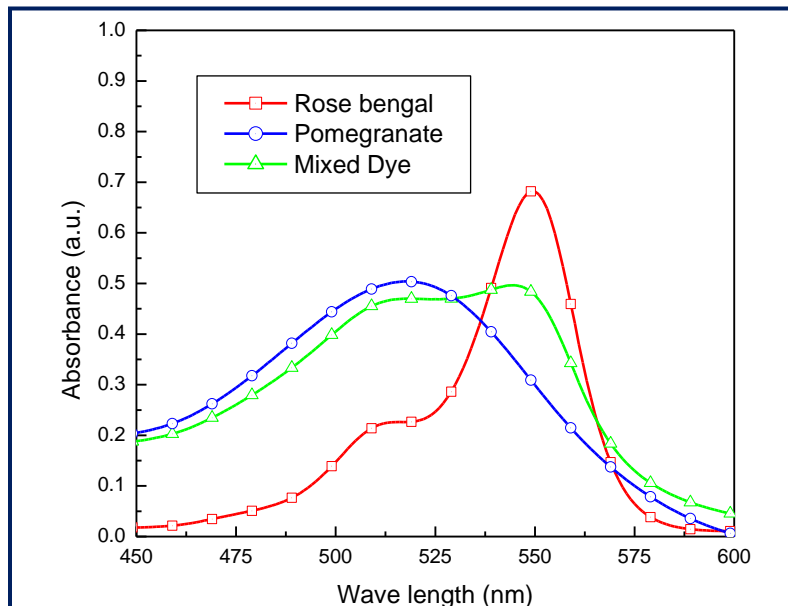


Figure 5-6 Absorption spectra of Rose Bengal, Pomegranate and Mixed dye

The peak of the absorption spectra of the dyes are in tune with HOMO-LUMO energy difference of Xanthene and Anthocyanin class of dye. Since no single dye can perform efficiently in the entire visible spectrum, the present work is focused on the performance study of *I-V* curve of DSSCs with various dyes having broadband absorption in the visible spectrum for efficient harvesting of light by DSSCs. The Rose Bengal dye absorbs a larger fraction of the solar spectrum in the visible region 460–650 nm. The Rose Bengal dye has been used to sensitize ZnO electrode of the DSSCs. On the other hand, Pomegranate is a natural dye with wider absorption peak at lower wavelength range of solar spectrum. The spectrum of mixed dye shows even wider absorption band and is expected to harvest more solar energy.

5.2.5 Performance of the DSSC

We have recorded *I-V* characteristics of ZnO nanorods based DSSCs using Rose Bengal, Pomegranate (*Punica Granatum*) and Mixed dye with equal proportion mixture of these two, with varied external resistances under illumination.

Figure 5-7 shows the current voltage curves of various dyes based on DSSCs solar cells. The Rose Bengal dye shows highest short circuit current whereas Pomegranate has lower value of both open circuit voltage and short circuit current. However, the mixed dye showed highest open circuit voltage with appreciable short circuit current.

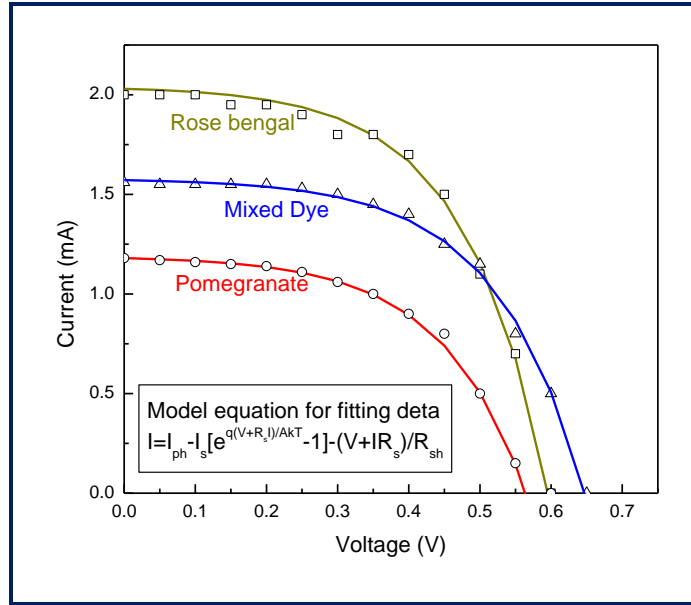


Figure 5-7 Current-voltage curves of various dyes based DSSC

5.2.6 Photovoltaic Properties

The open-circuit voltage (V_{oc}), short circuit current (I_{sc}), maximum voltage (V_{max}), maximum current (I_{max}), values of DSSC cells with three different dyes were calculated from Figure 5-7 and fitted with the Equation 5-3 for one diode equivalent circuit model (Figure 5-5) by Newton-Raphson's method. Results of Curve fitting were given in Table 5-2.

The parasitic resistances (series and shunt) of DSSCs are important parameters that affect its efficiency. The resulting parasitic resistances, series (R_s) and shunt resistance (R_{sh}) were evaluated from these results. Pomegranate has high series resistance, whereas using mixed dye we get subsequent reduction in series resistance, which results in substantial improvement in cell performance. Form the data of Table 5-2, it was confirmed that for all kinds of cells, higher the shunt resistance, the efficiency is lowered and efficiency raises with lower series resistances. The fill factor (FF) for all the cells using different dyes are also evaluated from the I-V characteristics using equation (5-1) and finally the energy conversion efficiency (η) is calculated using equation (5-2). All these results are presented in Table 5-2.

All cell parameters like Ideality Factor (A), Fill factor (FF) and Energy conversion efficiency (η) of ZnO based DSSCs with different dyes were calculated and presented in Table 5-2 where values are calculated from current voltage curves of DSSC cells fabricated with various dyes.

Table 5-2 Solar cell parameters of the three DSSCs

ZnO DSSC Dyes	V _{oc} (V)	I _{sc} (mA)	I _s (μ A)	R _s (Ω)	R _{sh} (Ω)	A	FF	η (%)
Rose Bengal	0.61	2.10	13.26	0.00308	3461	4.55	0.49	1.56
Pomegranate	0.56	1.18	9.88	0.00489	5011	4.57	0.56	1.01
Mixed Dye	0.65	1.57	7.96	0.00171	3934	4.73	0.54	1.41

The Rose Bengal dye shows highest efficiency and lowest fill factor, whereas Pomegranate shows lowest efficiency and highest fill factor. Though the mixed dye has an intermediate value of efficiency and fill factor, its values are very close to that of Rose Bengal. So, by mixing two kinds of dyes we achieved very good efficiency, which may be due to exploitation of wider band of energy in the solar spectrum as found out by the UV-VIS spectroscopic results of the mixed dye. This improvement in efficiency of the mixed dye is due to the improvement in ideality factor. Ideality factor indicates perfectness of the diode in the equivalent circuit, and it is 1.0 for a perfect diode. In our observation an improvement in ideality factor was observed, 4.73 for mixed dye, compared with 4.55 and 4.57 of pure dyes.

5.3 Gas Sensor

5.3.1 Response characteristics

The response characteristics of semiconducting ZnO film in the Whetstone bridge circuit showed distinct change in measured off-balance voltage with

infused tea leaves of different kinds when compared with the response in plain boiling water. A typical response curve with two different kinds of tea leaves, CTC and Orthodox tea, are presented in Figure 5-8. The difference in response with tea as compared with pure water is quite substantial. This shows that the effect of VOC's on sensor response is quite high. The high response is due to porous nanostructure of ZnO. The pore sizes of the nanostructured sensing element may be close to the organic molecules and so the adsorptions of these molecules are greatly intensified. This also imparts selectivity to some molecules. The molecules whose dimensions matches with that of the pores are adsorbed more resulting in higher response.

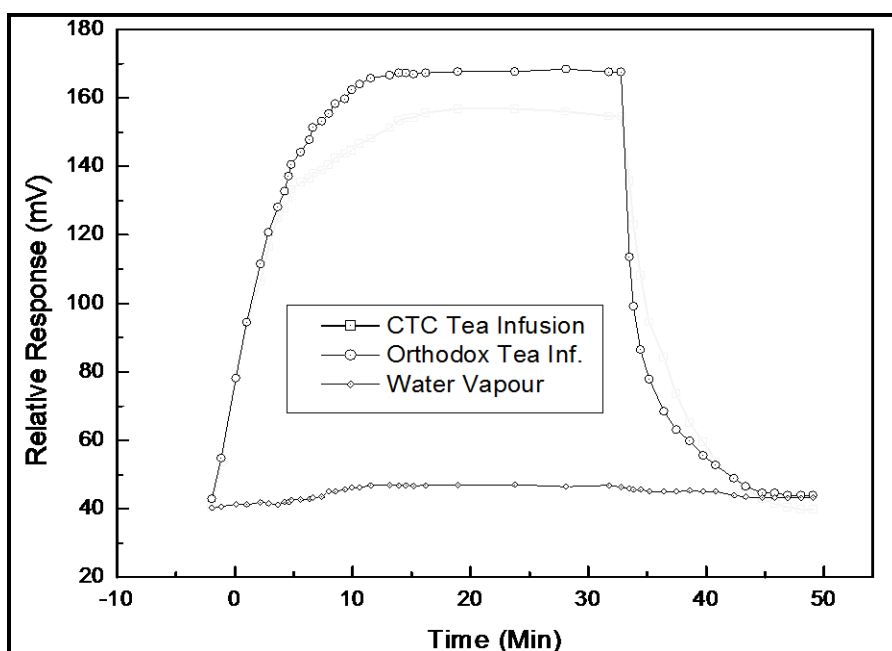


Figure 5-8 Response of the ZnO nanowire gas sensors

The gas sensors responses were measured at temperature 200°C with orthodox tea and CTC tea infusion (at 100°C) and compared with response in plain water vapour. Results show slightly lower concentration of VOC is detected for CTC compared to Orthodox tea which is in accordance to Tea taster reports that indicates Orthodox tea has superior flavour characteristics. The difference may be due to the presence of less VOC's in CTC leaves.

5.3.2 Response sensitivity with operating temperature

The sensor operating temperature is varied by controlling the heater current in the coil attached to the substrate. Results are presented in Figure 5-9 for two kinds of infusions. It shows that while the tea infusion temperature being the boiling point of water (100°C), that maximum sensitivity is obtained at around 100-200°C.

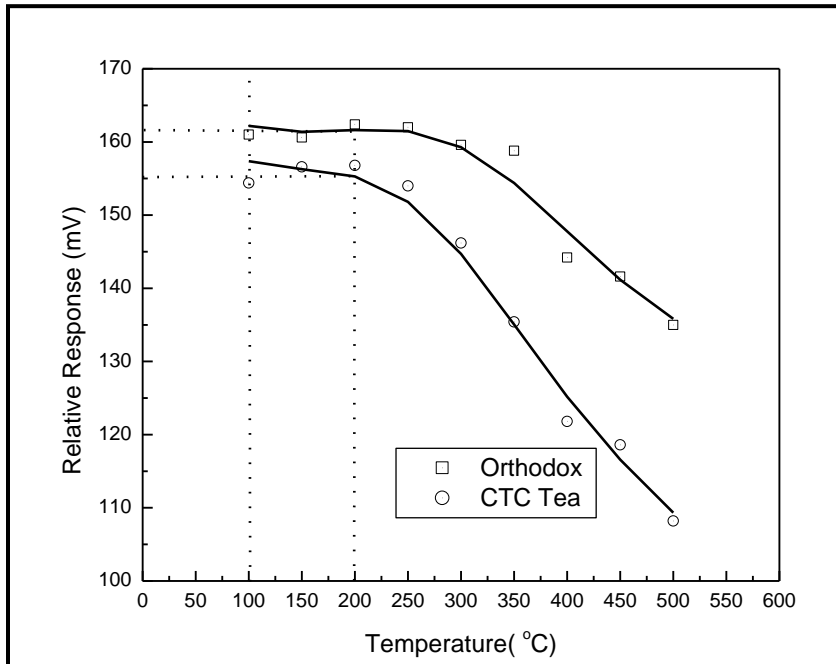


Figure 5-9 Orthodox tea and CTC with varying temperature

It shows that the sensitivity remains constant up to around 250°C and decreases beyond this temperature. Lowering of sensitivity with higher temperature could be explained due to following fact that adsorption of VOC molecules over nano-porous sensor substrate is reduced at elevated temperatures. The little rise in response for the range 100°C to 200°C can be due to higher mobility of VOC components.

5.3.3 Measurement of sensor characteristics

The sensitivity, response time and signal-to-noise ratio of two kinds of tea infusion are presented in Table 5-3. The sensitivity of ZnO based nanosensor is defined as:

$$S = \frac{(R_g - R_a)}{R_a} = \frac{\Delta R}{R_a} \quad 5-5$$

where R_a and R_g are the resistance of the sensing film in the atmosphere to be measured and the atmosphere that are referenced, respectively. In our case percentage change in output voltage can give an indication of sensitivity of the sensing system. Response time is the time taken by the sensing element to reach 90% of the final stable value of the response while the Signal-to-noise ratio was measured by the signal response divided by the mean fluctuation of results from its average value.

Table 5-3 Sensor Characteristics of ZnO VOC Sensor

Type of tea	Sensitivity (%)	Response time (Sec)	Signal-to-Noise Ratio
Orthodox	12.0	540	127
CTC	13.0	600	64

It was observed that sensitivity of CTC tea is higher than that of Orthodox tea. However, the Orthodox tea has got faster response. The signal-to-noise ratio for Orthodox tea leaves has got higher value than that of CTC tea. The differences in sensitivity are due to different types of organic molecules vaporized for different types of tea leaves. The response time is related to the vapourization rate of organic molecules concerned. At same temperature, different organic molecules vaporize at different time. As the VOC compositions of different types of tea are different, the vaporization rates of VOC's are different, resulting in differences in response time.

5.3.4 Doped ZnO Materials for Four Different Sensors

Tea is a non-alcoholic beverage consumed worldwide with an endlessly extending market. Like other food items, it also needs to be passed through the food safety and quality criteria [190]. Professional tea tasters have been traditionally assessing the physical quality attributes of tea by visual and nose approximations, which suffer from inconsistency and variability. So, there is a need for more accurate quality evaluation system [191]. Bio-chemical methods are available for assessment of tea quality applying modern analytical tools like high-performance liquid chromatography, gas chromatography, etc which are more accurate than human assessments, but these are time-consuming, and the results are often inconsistent with sensory evaluation. An application of electronic nose and vision coupled with multivariate data analysis in the analysis of foodstuffs has been increasing in last few years. The electronic testing devices are comprised of three principal components, sensor array, the equipment receiving signals and pattern recognition. In place of a single sensor, an array of sensors is solving the purpose more efficiently.

This is done by using array of sensors with partially overlapping selectivity and treating the data obtained by multivariate methods. E-noses have been used for identification of tea grade, prediction of tea quality, and monitoring of black tea fermentation process [192]. E-nose devices have also been successfully applied to different fields particularly in food and beverage industries, such as tomato, and coffee [193]. Computer vision systems are also gaining significant popularity in food industry because of their cost effectiveness, consistency, superior speed and accuracy. Also, the methods used so far for estimation of tea quality parameters have their own merits and demerits as they have been developed independently [191]. In the present study, an attempt has been made to integrate the three types of tea quality measurement techniques viz., taster's scoring, biochemical analysis and electronic sensor based studies, to find a correlation between them. This

would be used to standardize the electronic sensor based study of Darjeeling Orthodox black tea quality, to contribute to the process of simplification as well as enhancing accuracy in determination of tea quality.

5.3.5 E-nose Application of Doped ZnO Sensors for Tea Quality Estimation

The E-nose was developed in order to mimic human olfaction that functions as a non-separative mechanism: i.e. an odor / flavor is perceived as a global fingerprint. Essentially the instrument consists of head space sampling, sensor array, and pattern recognition modules, to generate signal pattern that are used for characterizing odors.

Electronic noses include three major parts: a sample delivery system, a detection system, a computing system. The sample delivery system enables the generation of the headspace (volatile compounds) of a sample, which is the fraction analyzed. The system then injects this headspace into the detection system of the electronic nose. The sample delivery system is essential to guarantee constant operating conditions.

The detection system, which consists of a sensor set, is the "reactive" part of the instrument. When in contact with volatile compounds, the sensors react, which means they experience a change of electrical properties.

In most electronic noses, each sensor is sensitive to all volatile molecules but each in their specific way. However, in bio-electronic noses, receptor proteins which respond to specific odor molecules are used. Most electronic noses use sensor arrays that react to volatile compounds on contact: the adsorption of volatile compounds on the sensor surface causes a physical change of the sensor. A specific response is recorded by the electronic interface transforming the signal into a digital value. Recorded data are then computed based on statistical models [194].

In our case, there are four sensors and there are various Volatile Organic Components arising in tea infusion has to be detected. The contribution to

individual gas component can be isolated through Principal Component Analysis (PCA).

5.3.6 Principal Component Analysis

PCA reduces the data dimension to some principal components and enables the extraction of the differences between samples and the main variables. The data of 51 samples were analyzed by PCA. PCA is a linear method that has been proved to be effective for discriminating the response of gas sensor array to simple and complex odours. Considering the differences of sensitivities of gas sensors, all data have been normalized before analyzed by PCA. Figure 5-10 shows PCA results of training data set projected onto their first two principle components.

Table 5-4 Covariant Matrix formed from responses of four different sensor and its Eigen values

(a) The Covariant Matrix

0.0025	0.0013	0.0087	0.0141
0.0013	0.0011	0.0035	0.0056
0.0087	0.0035	0.0455	0.0669
0.0141	0.0056	0.0669	0.1170

(b) Eigen values of Covariant Matrix

Eigenvalue-1	Eigenvalue-2	Eigenvalue-3	Eigenvalue-4
0.1592	0.0054	0.0014	0.0002

Four eigenvalues of covariance matrix are listed in Table 5-4 (b). It was found that the first eigenvalue appears to be the largest and other eigenvalues are smaller by an order of 10^2 . Therefore, the response data were greatly aligned along first principal component. In other words, the aroma in Darjeeling Orthodox tea liquor arises mostly from a single component. This is also evident from the PCA result shown in Figure 5-10. Where all data were mostly aligned in the direction of first principle component.

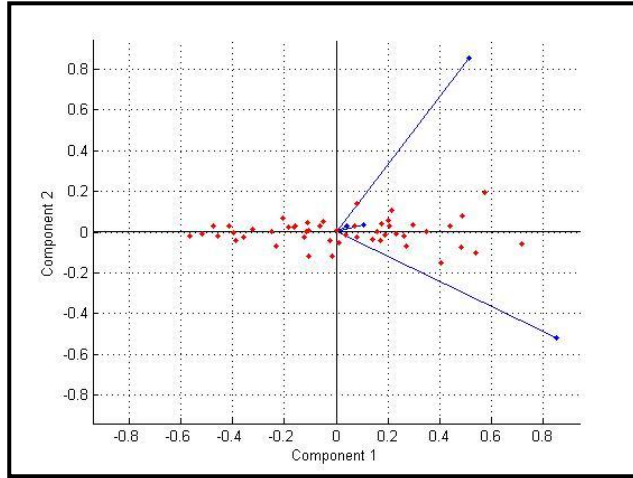


Figure 5-10 PCA results of training data obtained from sensor array.

5.3.7 Development of E-Nose response function

Response of individual sensors will have either positive correlation or negative correlation with individual flavour component. i.e. some sensors have positive response with a particular flavour component, whereas, some exhibits negative response. Also, the contribution of individual response due to flavour component will be proportional to the sum for a particular sensor's response [195]. So, a function is constructed for the total sensor response (S) which is a linear sum of individual response multiplied by the individual gradient value of each sensor response.

$$S = \sum_{i=1}^4 R_i \times |M_{si}| \quad 5-6$$

where, M_{si} ($i = 1$ to 4) is the individual response of each attributes factor, and R_i is the weight coefficient corresponding to each attribute. The gradients of individual responses are taken as the weight coefficient of that sensor element.

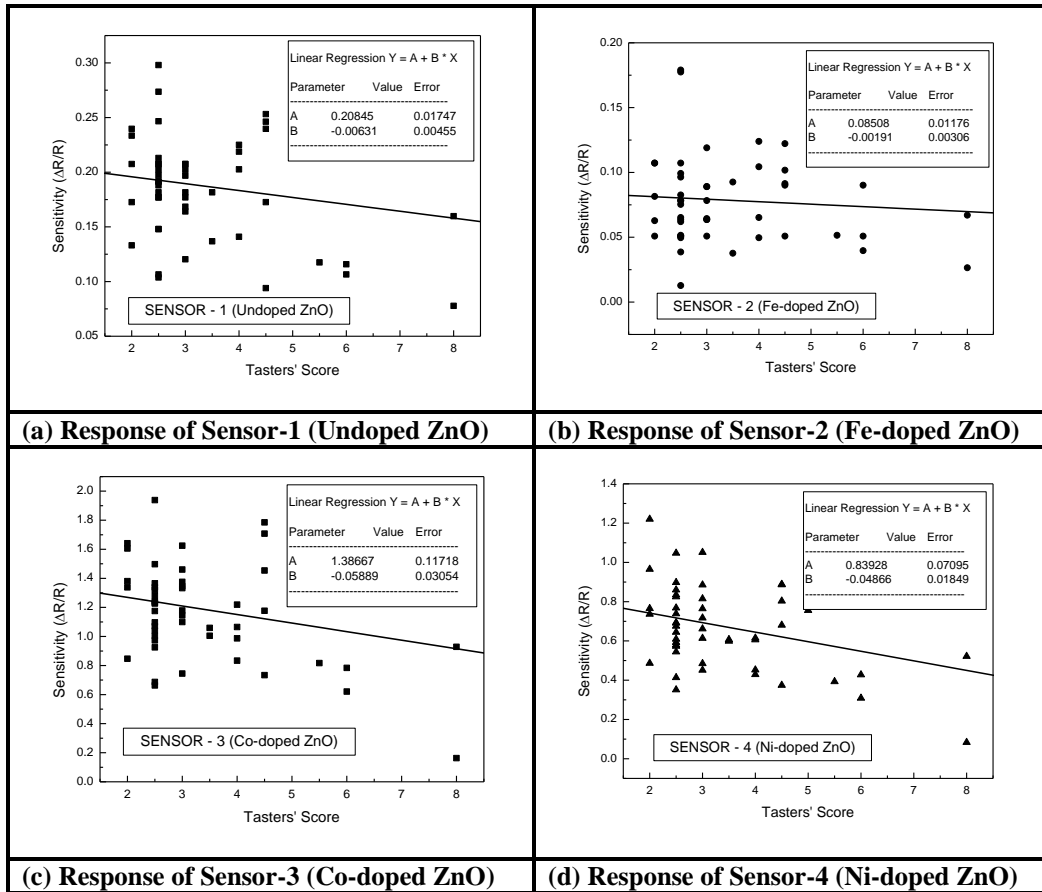


Figure 5-11 Calculation of individual response gradient of four different sensor elements.

The response from each sensor is plotted with tasters flavour score and the gradient is noted and presented in Table 5-5.

Table 5-5 Gradient of each sensor calculated from individual response.

Sensors	Un-doped	Fe-doped	Co-doped	Ni-doped
Response (R_i)	R_1	R_2	R_3	R_4
Gradient (M_{Si})	-0.00631	-0.00191	-0.04866	-0.05889

The resulting function is plotted with the Taster's scores obtained for orthodox tea. Figure 5-12 shows the calibration of the sensors using a new function built appropriately from individual sensor responses as presented in

Equation 5-5 where the weight coefficient of four individual sensing elements was built through multiple regression equation of four sensor data versus the tasters flavour score.

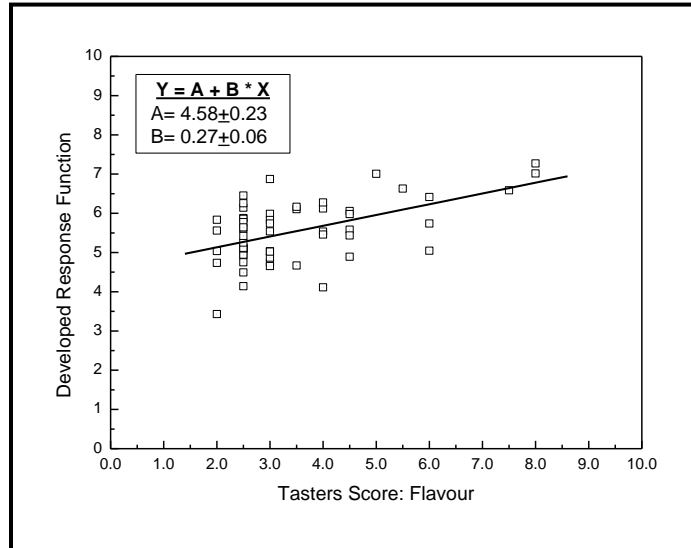


Figure 5-12 Calibration of the sensors using a function built from individual sensor responses for Orthodox black tea.

When this newly developed function is plotted with the tasters' flavour score, a very good linear relationship is observed with very small scattered data exhibiting a significantly high value of the gradient as presented in Figure 5-12.

CHAPTER 6

6. SUMMARY AND CONCLUSION

Fe, Co and Ni doped ZnO thin films were prepared by the sol-gel method. All films were oriented preferentially along the (0 0 2) direction. Films doped with 1 at.% iron concentration, 1 at.% cobalt and 1 at.% nickel for each dopant had a stronger c-axis orientation perpendicular to the substrate, larger grain, more smooth surface morphology and higher conductivity and transmittance than the others. The iron doped film with 1 at.% had a thickness of 200 nm and a columnar structure. The thicknesses of films doped with 1 at.% cobalt concentration and 1 at.% nickel were 250 and 200 nm, respectively, and these films had a round particles of different sizes. High conductivities and transmittances were shown in the preferred (0 0 2) oriented films. In particular, the iron doped ZnO film with 1 at.% reached an electrical resistivity value of $1.1 \times 10^{-1} \Omega\text{-cm}$, while a transmittance of over 90% in the visible range was achieved.

ZnO nanorod based DSSC solar cells structure was fabricated on an ITO coated glass substrate and the cell performance of ZnO-based DSSCs was found out for two types of dyes and also for their mixture. The dyes differ in their absorption spectra and absorb sunlight in different frequency range. The mixed dye with larger band of frequency spectrum shows improvement in efficiency than the average efficiency of the two dyes. This improvement in efficiency of the mixed dye is due to the improvement in ideality factor.

The ZnO nanorods based DSSCs were synthesized on ITO coated glass substrate by the sol-gel spin coating technique. For developing the sensitizer, natural dyes were extracted from locally available fruits. The dyes strongly absorb visible light having wavelength lying in region 450 and 600 nm. The equivalent circuit parameters of natural dye based DSSCs which determines

the performances in DSSC were calculated. The efficiency of ZnO nanostructures based DSSCs was closely related to the various natural dyes. The DSSC cell efficiency has been calculated natural dye based solar cells. Higher electrical conductance in the ZnO film and appropriate dyes and electrolytes are needed to improve the DSSC efficiency. These types of fabrication at low cost can also improve efficiency performance of natural dye based DSSCs by using liquid electrolyte KI₃. A study of parasitic resistance parameters (R_s and R_{sh}) of DSSCs from I - V curve using the equivalent circuit one-diode model were presented.

Nanostructured sensing element of ZnO was fabricated on glass substrate. The microstructure shows neat columnar structure with uniform porosity. X-ray diffractogram shows formation of pure ZnO phase. The nanostructured ZnO film showed distinct change in their resistivity with infused tea leaves of different types. Due to its characteristic pore structure organic gas molecules are adsorbed over sensing surface resulting in selective response with different types of tea. Sensitivity of Orthodox tea was found to be lower than that of CTC tea which may be due to the more number of flavory VOC's in Orthodox tea infusion. The response time and signal-to-noise ratio in Orthodox tea are also better than CTC tea.

Zinc Oxide nanorods were successfully synthesized for the application of nanostructured sensing element. Also the Doped Nanostructured Zinc Oxide materials were prepared with difference in characteristics like, resistivity, band gap etc.

In order to design a cost effective solution, a natural dye based DSSC was fabricated and evaluated using the existing indoor experimental data to predict the performance of ZnO nanorod-based DSSC. All the device characteristics of the fabricated DSSC device was calculated.

Sensing elements using the doped Zinc Oxide sensing elements with varying characteristics like, resistivity, band gap etc. was fabricated which are expected to impart selectivity in sensing elements. Sensors fabricated were tested in Orthodox Tea infusion which shows specific selectivity of the Volatile Organic Components when Principal component analysis was performed. The results were correlated with Tea Tasters Flavour quality assessment through multiple linear regressions. Subsequently a methodology was developed and calibrated for estimation of tea flavour quality for Orthodox Tea

CHAPTER 7

7. RECOMMENDATION AND FUTURE WORK

The semiconducting ZnO thin film sensor is a promising candidate for sensor development because of its selectivity to many gases i.e. VOC gases of interest and the ability to be integrated with IC-based nano-technology. However, the fundamental understanding of sensing properties of ZnO based thin film sensor remains poor since an empirical optimization of sensor performance has focused on the use of simple DC resistance measurements. In continuation with present work, other types of nanostructured materials like TiO₂ can be tested with natural dyes for the performance of DSSC device.

The effort to understand the DSSC performance of ZnO thin film has been pursued using I-V characteristics and Dye absorption spectra by UV-Vis spectrometer. In this study, a ZnO based DSSCs using natural dyes were studied and investigated. While consistent models explaining the source of the field-induced drift were proposed, additional studies are required to define these processes more precisely. Suggested studies include (1) estimating the characteristics of ion/charge migration using relaxation techniques and microelectrodes, (2) investigating the electrical profile between electrodes, (3) studying the major role of natural dyes between the electrodes (4) in diffusion studies to establish electron/ hole exchange and (5) pursuing schemes to prevent or reduce the parasitic resistances inside the DSSCs in presence of light.

Further investigations are required to identify superior low cost natural dyes that have higher molar excitation coefficients, broad UV-Vis absorption range, chemical and thermal stability in order to optimize photoelectrochemical solar cell for liquid electrolyte based DSSCs. More

natural dyes may be tested to find the appropriate one with better device characteristics.

The recent reports show an encouraging breakthrough in improvement of efficiency for natural dye based solar cells. However, there is a common problem for all the application of such cells: stability. Hence to our opinion, an extensive indoor/outdoor experimental study for the improvement of stability of natural dye based solar cells may be performed.

Further investigation is under progress to fine tune the response of the two types of tea leaves by changing the size of the microstructures and also by doping ZnO film with appropriate materials. Single MEMS design of the tested E-nose can be designed and fabricated to test and measure the flavour quality of Orthodox black tea.

